Review

Sensing Performances of Hierarchical Nano-Layered V_2O_5 Structures and *Ab Initio* Calculation of Their Gas-Adsorption Properties

Vuyani Sifunda , Olatunbosun Nubi , Evans Benecha , Bonex Wakifwa Mwakikunga , Amos Adeleke Akande *

Posted Date: 4 February 2026

doi: 10.20944/preprints202602.0309.v1

Keywords: nano layered; hierarchical structure; gas sensors; DFT; V_2O_5; adsorption energy

 doi:10.20944/preprints202602.0309.v1

Review

Sensing Performances of Hierarchical Nano-Layered V_2O_5 Structures and *Ab Initio* Calculation of Their Gas-Adsorption Properties

Vuyani Sifunda [1,2], Olatunbosun Nubi [2], Evans Benecha [3], Bonex Wakifwa Mwakikunga [4,5] and Amos Adeleke Akande [1,6,*]

[1] CSIR Nextgen Enterprises and Institutions, P O Box 395, Pretoria 0001, South Africa
[2] University of Limpopo, Department of Physics, P/Bag X1106, Sovenga 0727, South Africa
[3] Department of Physics, University of South Africa, UNISA 0003, Pretoria, South Africa
[4] DST/CSIR National Centre for Nano-Structured Materials, P O Box 395, Pretoria 0001, South Africa
[5] Department of Physics, Tshwane University of Technology, Private Bag 68, Pretoria, 0001, South Africa
[6] Department of Mathematical and Physical Science, School of Computing, Engineering and Mathematical Sciences, La Trobe University, Bundoora, VIC 3086, Australia
* Correspondence: amos.akande@sydney.edu.au

Abstract

Significant research efforts have recently focused on nanomaterial processing for gas sensors and related sensing applications. However, the major challenges in the field involve the choice of material for the sensing layer of the sensor device element together with the right structure, assembly, and morphology through which the full sensing properties of the material can be realised. Herein, we critically review the hierarchical nanostructures of V_2O_5 nanomaterial for application in gas sensing technology. Beyond the sheet structure which serves as the fundamental building block of the V_2O_5'smolecular arrangement, Nanostructures ranging from nanobelts to nanowires, nanorods, nanoribbons, nanofibers, nanotubes, and thin films were discovered as preferred configuration and thermodynamically favorable structures – according to many synthesis processes. Ethanol (C_2H_5OH) and Nitrogen dioxide (NO_2) gases were identified as preferred molecules commonly detected by various V_2O_5 morphologies, with the nanotube structure showing preferential sensitivity and selectivity to C_2H_5OH. We also discuss perspectives from density functional theory (DFT) studies of V_2O_5 nanostructures and other (2D) materials structures for gas sensing applications. The studies highlight enhanced adsorption energy, increase conductivity, and band gap variation as a result of an upper shift in Fermi level, all as consequence of surface interaction between semiconductor crystal orientation and chemical molecules. Finally, our calculations of the optimised parameters for α-V_2O_5 orthorhombic structure showed good agreement with experimental and other theoretical data in the literature. The adsorption energy profile for NO_2 molecules revealed that Ag-doped surface exhibits the most negative adsorption energy compared with the clean surface and other doped surfaces.

Keywords: nano layered; hierarchical structure; gas sensors; DFT; V_2O_5; adsorption energy

1. Introduction

The release of these toxic gases (NO, SO_2, CO, CO_2, SO_2, H_2S, and NH_3) from chemical industries, mines, and power plants has put a strain on the health of human beings, resulting in cardiovascular illnesses such as asthma, arrhythmia, and heart failure etc.), especially in pregnant women and elderly people. Moreover, these toxic gases and volatile gases have also contributed immensely to climate change resulting in extreme weather occurrences. The demand for highly efficient, reliable, and low-cost gas sensors has increased tremendously all over the world in recent years. With the advances of the fourth industrial revolution in bridging gaps between the field of science and

 doi:10.20944/preprints202602.0309.v1

technology, nanotechnology has been marked to be a major player among 4.0 emerging technologies. Nano gas sensors have gained extensive use in the medical field, to diagnose diseases and identify the nature of illness through monitoring the exhaled breath of patients. However, the most reliable and highly recommended technique for gas detection nanoparticle-based materials is to be considered, especially in the medical field for long-term health purposes.

The release of toxic gases (e.g., NO, SO_2, CO, CO_2, H_2S, and NH_3) from chemical industries, mines, and power plants poses a significant threat to human health, leading to cardiovascular illnesses such as asthma, arrhythmia, and heart failure, particularly among pregnant women and the elderly. Furthermore, these toxic and volatile gases contribute immensely to climate change and extreme weather events. Consequently, global demand for highly efficient, reliable, and low-cost gas sensors has increased tremendously in recent years.

Advancements linked to the Fourth Industrial Revolution, which bridges science and technology, have positioned nanotechnology as a major player among emerging Industry 4.0 technologies. Nano gas sensors are now extensively used in medicine to diagnose diseases and identify illnesses by monitoring patients' exhaled breath [5–8]. For reliable, long-term health monitoring, nanoparticle-based materials are considered a highly recommended technique for gas detection.

The use of metal oxide semiconductors (MOS) materials for the development of gas sensors can be dated back to 1954 and has continued to be one of the most effective techniques in monitoring the concentration of gases in the atmosphere. Nano MOS materials like SnO_2, ZnO, WO_3, V_2O_5, Fe_2O_3, and TiO_2 are widely investigated for gas sensor applications because of their high surface to volume ratio, low manufacturing cost, and capability of detecting a large number of toxic gases at different temperature. The sensing mechanism of these MOS materials lies in the changes in electrical conductivity upon exposure to a concentration of gases due to catalytic reduction/oxidation reactions occurring at the oxide surface. In recent years, gas sensors based on 2-dimensional structures (2D)-such as vanadium pentoxide (V_2O_5), molybdenum disulphide (MoS_2), tungsten disulphide (WSe_2), hexagonal boron nitride (h-BN), Carbon materials, and graphene nanostructures have been attracting tremendous attention for gas sensor fabrication.

The use of metal oxide semiconductor (MOS) materials for gas sensor development dates back to 1954 and remains one of the most effective techniques for monitoring atmospheric gas concentrations. Nano-MOS materials such as SnO_2, ZnO, WO_3, V_2O_5, Fe_2O_3, and TiO_2 are widely investigated for gas sensing due to their high surface-to-volume ratio, low manufacturing cost, and capability of detecting numerous toxic gases at different temperatures. The sensing mechanism of these materials relies on changes in electrical conductivity upon exposure to target gases, driven by catalytic reduction/oxidation reactions at the oxide surface. Recently, gas sensors based on two-dimensional (2D) structures—such as vanadium pentoxide (V_2O_5), molybdenum disulphide (MoS_2), tungsten disulphide (WSe_2), hexagonal boron nitride (h-BN), carbon materials, and graphene nanostructures—have attracted tremendous attention for sensor fabrication.

Among various 2D-based structures, V_2O_5 is an upcoming gas-sensing material because of its low optical bandgap of 2.5 eV, and excellent thermal and thermoelectric properties relative to other semiconducting metal oxides. This material is among the top 10 most researched oxides. Moreover, this material is considered the most stable among other vanadium oxide members such as vanadium monoxide (VO), vanadium dioxide (VO_2), and vanadium sesquioxide (V_2O_3). V_2O_5 possesses different polymorphs namely α-V_2O_5 (orthorhombic), metastable β-V_2O_5 (tetragonal or monoclinic), γ-V_2O_5 (orthorhombic), and δ-V_2O_5 (monoclinic) with each being stable at different temperature and pressure. α-V_2O_5 is the most commonly used material for gas sensing applications compared to the other polymers. This material exhibits Mott Hubbard's metal-to-insulator (MTI) at a given temperature (375°C). Its unique crystallographic unit cell structure, electronic properties, high surface area to volume ratios, and several reaction sites enable it to exhibit high selectivity and response towards different gases.

 doi:10.20944/preprints202602.0309.v1

Among various 2D-based structures, V_2O_5 is an emerging gas-sensing material owing to its low optical bandgap (~2.5 eV) and excellent thermal and thermoelectric properties compared to other semiconducting metal oxides [1–3]. It ranks among the top ten most researched oxides [4] and is considered the most stable member of the vanadium oxide family, which includes vanadium monoxide (VO), vanadium dioxide (VO_2), and vanadium sesquioxide (V_2O_3) [5]. V_2O_5 exhibits several polymorphs, including α-V_2O_5 (orthorhombic), metastable β-V_2O_5 (tetragonal or monoclinic), γ-V_2O_5 (orthorhombic), and δ-V_2O_5 (monoclinic), each stable under different temperature and pressure conditions [6,7]. The α-V_2O_5 phase is the most commonly used for gas sensing and exhibits a Mott–Hubbard metal-to-insulator transition (MTI) at approximately 375 °C [8,9]. Its unique crystallographic structure, electronic properties, high surface-area-to-volume ratio, and abundant reaction sites enable high selectivity and sensitivity toward various gases [10–14].

Research has shown that different atomic arrangements or structures of semiconducting materials called hierarchical structures, often result in different chemical, optical-electronic, magnetic, etc. properties [15,16]. This has also been demonstrated in the case of gas and chemical sensing where hierarchical structures of materials exhibited different adsorption properties (surface areas, pores volumes, and pore diameters) which consequently yielded different sensitivity, response time, recovery time, and gas selective ability [17–19]. For instance, the large surface area of WO_3 hierarchical structures has been said to provide more channels which not only make gas diffusion great but also allow more active sites for adsorbing gases, thus leading to high gas sensing performance [19]. Higher gas response of SnO_2 nanoneedles with quicker response and recovery of the same material when in nanosheets assemble was reported [20]. The high response property of the nanoneedles structures is attributed to the large surface area from the Brunauer-Emmett-Teller (BET) test. More adsorption and desorption sites were also reported for nanoneedle structures which allowed gas molecules to easily diffuse across the surface. Spacing among the nanosheets is large (compared to an open room) relative to nanoneedles which give high pores for quicker response and recovery. Other reports have also shown that nanowires are the most researched morphology with 40%, followed by nanobelts and nanorods with 20%, nanotubes with 20%, and nanobelts with 20% [4].

Research has shown that hierarchical structures—different atomic arrangements or assemblies of semiconducting materials—can lead to distinct chemical, optoelectronic, and magnetic properties [15,16]. This principle also applies to gas and chemical sensing, where hierarchical morphologies influence adsorption properties (e.g., surface area, pore volume, pore diameter), thereby affecting sensitivity, response time, recovery time, and selectivity [17–19]. For instance, the large surface area of WO_3 hierarchical structures provides more channels for gas diffusion and additional active sites for adsorption, leading to enhanced sensing performance [19]. Similarly, SnO_2 nanoneedles have demonstrated higher gas response, while SnO_2 nanosheet assemblies enable quicker response and recovery [20]. The improved performance of nanoneedles is attributed to their large BET surface area, which offers abundant adsorption/desorption sites and facilitates gas molecule diffusion on the materials 'surface. In contrast, the wider spacing between nanosheets creates more open pores, promoting faster response and recovery. Reports indicate that nanowires are the most researched morphology (≈40%), followed by nanobelts, nanorods, and nanotubes [4].

It has been reported that the hierarchical hollow structure of Zinc stannate ($ZnSnO_3$) composed of ultra-thin nanorods as building blocks has shown fast response and recovery capacities, and good repeatability in the detection of ethanol. This is related to the hollow structure having efficient surface area and surface accessibility [21]. Due to these exceptional properties, $ZnSnO_3$ shows permeable surfaces that allow easy absorption of ethanol gas molecules [22] resulting in a fast response. Zinc oxide (ZnO) nanorod is another unique material that exhibits a quicker response and recovery speed towards ethanol detection, as compared to nanosheets which display a larger ethanol response. The quicker response of ZnO nanorod is due to its better conductivity and lower potential barrier, while the larger response of nanosheets results from its higher specific surface area [23]. Other studies have also reported that hierarchical and hollow Indium oxide (In_2O_3) material has shown higher response

 doi:10.20944/preprints202602.0309.v1

and recovery times as compared to its agglomerated counterparts (powder) in the detection of carbon monoxide (CO) [24]. This is a result of its structural assembly which allows effective and rapid gas diffusion toward the entire sensing surface. Metal oxide nanostructures/Porous Silicon (PS) composites, such as PS/WO_3 [25] and PS/ZnO [26,27] have been reported to show good sensing abilities towards different gases. PS/V_2O_5 nanorod composite material exhibits high response and good selectivity towards NO_2 at room temperature [28]. The porous silicon provides a high surface-to-volume ratio in composites (PS/V_2O_5) while the nanorods have specific surface areas and dimensions comparable to Debye length. The heterojunction between the two helps the material in achieving good sensing performance [28].

Hierarchical hollow structures also show promise. For example, zinc stannate ($ZnSnO_3$) composed of ultrathin nanorod building blocks exhibits fast response/recovery, good repeatability, and efficient ethanol detection due to its high surface area and accessibility [21,22]. Zinc oxide (ZnO) nanorods demonstrate quicker response and recovery toward ethanol compared to nanosheets, owing to better conductivity and a lower potential barrier, whereas nanosheets show a larger response due to their higher specific surface area [23]. Hierarchical and hollow indium oxide (In_2O_3) structures exhibit higher response and faster recovery times than their agglomerated powder counterparts in carbon monoxide (CO) detection, a result of their assembly promoting effective and rapid gas diffusion [24].

Metal oxide nanostructure/porous silicon (PS) composites, such as PS/WO_3 [25] and PS/ZnO [26,27], have also demonstrated good sensing abilities. Notably, a PS/V_2O_5 nanorod composite exhibits high response and good selectivity toward NO_2 at room temperature [28]. In such composites, porous silicon provides a high surface-to-volume ratio, while the nanorods offer specific surface areas and dimensions comparable to the Debye length. The heterojunction between the two materials further enhances sensing performance [28].

Having established that the morphologies or structures of metal oxide nanomaterials have a relationship with the chemical, physical, and gas-sensing properties of a material, it is obvious that crucial information about the choice of gas-sensing materials can be obtained. It is then essential to critically review the structures of V_2O_5 for the benefit of exploring them for gas sensor development. Thus, this paper presents a systematic review of the sensing properties of V_2O_5 nanomaterials in hierarchical structure assembly.

Given the established relationship between morphology (hierarchical structure) and the chemical, physical, and gas-sensing properties of metal oxide nanomaterials, crucial insights can be gained for selecting optimal sensing materials. Therefore, a critical review of V_2O_5 nanostructures is essential to explore their full potential for gas sensor development. This paper presents a systematic review of the sensing properties of V_2O_5 nanomaterials with a focus on hierarchical structure assemblies.

 doi:10.20944/preprints202602.0309.v1

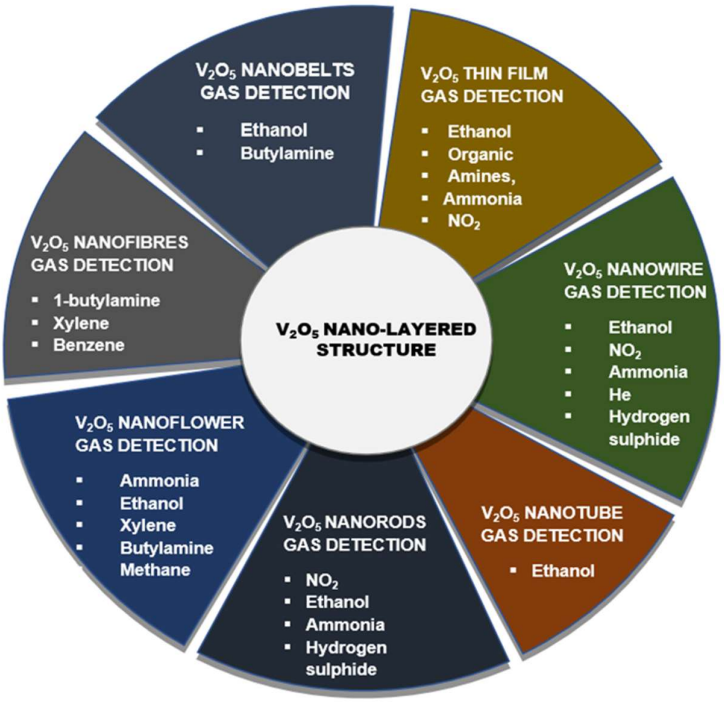

Figure 1. Summary of V_2O_5 morphologies with their possible detectable gases.

2. Hierarchical Nanostructures of V_2O_5

2.1. V_2O_5 Nanobelts

Vanadium pentoxide (V_2O_5) nanobelts are distinct metal oxide semiconductor nanoparticles that are in the form of a belt [29]. They are distinguishable from other morphologies such as nanotubes and nanowires by their rectangular cross-sectional area, which allows a complete understanding of dimensionally limited transport events at the nanoscale scale [30]. The V_2O_5 single crystalline nanobelts are often synthesised through the hydrothermal technique, which is a versatile and convenient process that allows full control of size, shape, and crystallinity [31,32]. This process often results in nanobelts that are highly uniform in size and shape. Their high porosity also makes them more suitable for the absorption of different species. Nanobelts possess good electrical conductivity, which allows them to be more useful in various applications such as solid-state batteries, supercapacitors, and gas sensors. However, in gas sensor applications, the fabricated gas sensors based on pristine V_2O_5 nanobelts have shown moderate response towards detecting gases such as ethanol and butylamine at different temperatures (Table 1). [33]. Many studies have suggested surface modification, through coating the surface of V_2O_5 nanobelt with noble metal nanoparticles as well as doping with transition metals, as an effective method to enhance the material sensitivity and stability [34].

Vanadium pentoxide (V_2O_5) nanobelts are distinct metal oxide semiconductor nanoparticles with a belt-like morphology [29]. They are distinguished from other morphologies, such as nanotubes and nanowires, by their rectangular cross-section, which facilitates the study of dimensionally confined transport phenomena at the nanoscale [30]. Single-crystalline V_2O_5 nanobelts are often synthesised via the hydrothermal technique, a versatile and convenient process that allows full control over size, shape, and crystallinity [31,32]. This method typically yields nanobelts with high uniformity in size and shape. Their high porosity enhances their suitability for absorbing various species. Nanobelts also possess good electrical conductivity, making them useful in applications such as solid-state batteries, supercapacitors, and gas sensors. However, in gas sensing, sensors fabricated from pristine V_2O_5 nanobelts have shown only a moderate response to gases such as ethanol and

 doi:10.20944/preprints202602.0309.v1

butylamine at different operating temperatures (Table 1) [33]. Consequently, many studies suggest that surface modification—through coating with noble metal nanoparticles or doping with transition metals—is an effective method to enhance sensitivity and stability [34].

Table 1. Summary of V_2O_5 nanobelts coated with TiO_2, $Fe2O_3$ and SnO_2.

Nanobelt Material	Operation temperature (°C)	Targeted gas	Concentration (ppm)	Response *	Response time/Recovery time	Reference
Pristine V_2O_5	250	Ethanol	100	1.7	32/30	[35,36]
V_2O_5/TiO_2	250	Ethanol	100	2.	49/85	[35,36]
V_2O_5/Fe_2O_3	250	Ethanol	100	2.3	36/64	[35,36]
V_2O_5/SnO_2	250	Ethanol	100	3.1	37/126	[36,37]
$Ag_{0.35}V_2O_5$	260	Ethanol	5-100	1	50	[38,39]

*Response $\frac{Rg-Ra}{Ra} * 100\%$ [39].

The surface of the V_2O_5 nanobelt has been reported to be significantly enhanced when coated with metal oxide nanoparticles such as SnO_2, TiO_2, and Fe_2O_3. This has been observed to increase the width and thickness of the sensing material by 60-100 nm and 10-20 nm, respectively, compared to the pristine V_2O_5 nanobelt. The sensitivity of the coated V_2O_5 nanobelt has been reported to be three times that of the pristine V_2O_5 nanobelt. This is attributed to the difference in sensing mechanism [34]. The adsorption process of the coated V_2O_5 nanobelt occurs primarily at the surface of the metal oxide. The smaller-sized nanocrystal grains of the coating metal oxide enable the adsorbed species to interact with all the atoms, resulting in the formation of a space-charged region that covers the entire metal oxide surface. The depth of the space-charged region is influenced by the oxygen ionosorption when the sensor is exposed to air. Upon exposure to a reducing gas such as ethanol, the adsorbed species react with ethanol, and electrons are released back into the surface of the sensor. These electrons travel through the metal oxide into the V_2O_5 nanobelt, resulting in conduction [35].

The surface properties of V_2O_5 nanobelts are reported to improve significantly when coated with metal oxide nanoparticles such as SnO_2, TiO_2, and Fe_2O_3. This coating increases the width and thickness of the sensing material by approximately 60–100 nm and 10–20 nm, respectively, compared to pristine V_2O_5 nanobelts. The sensitivity of the coated nanobelts can be up to three times higher, a difference attributed to a change in the sensing mechanism [34]. In the coated system, gas adsorption occurs primarily on the metal oxide surface. The small nanocrystal grains of the coating allow adsorbed species to interact with most atoms, forming a space-charge region that covers the entire metal oxide surface. The depth of this region is modulated by oxygen ionosorption when the sensor is in air. Upon exposure to a reducing gas like ethanol, the adsorbed species react, releasing electrons back to the sensor surface. These electrons then travel through the metal oxide into the V_2O_5 nanobelt, thereby increasing conduction [35].

2.2. V_2O_5 Thin-Films

The nanostructured vanadium oxide thin films are one of the metal oxides that possess variable optical properties and have been applied in a range of devices, including optical, catalysis, electrical switching, and gas sensing applications [40]. The functional properties of these thin films are highly

 doi:10.20944/preprints202602.0309.v1

influenced by several parameters such as surface area, crystallinity and the method or technique used for preparation [41]. There are several reported methods used for V_2O_5 thin film preparation, such as chemical vapour deposition [42], sol-gel method [43], and pulsed laser deposition [44,45]. Among them, pulsed laser deposition (PLD) has been reported to be an inexpensive and less energy-consuming process. This technique is capable of operating at a low temperature and has demonstrated advantages in the preparation of V_2O_5 films. These include easy control of the thickness and composition of the film by tuning the deposition parameters, as well as a good reproducible stoichiometry of the target material in the films for gas sensing applications [46]. In addition, this flexible and powerful method usually gives V_2O_5 thin films in various spherical sizes, with an average grain size of 50 nm and the surface roughness ranging from 9-20nm [47]. Reports have shown that V_2O_5 thin film demonstrates a good response towards oxidizing gases such as NO_2, organic amines, ethanol, and ammonia at different temperatures (Table 2).

Nanostructured vanadium oxide thin films are metal oxides with tunable optical properties, applicable in optical devices, catalysis, electrical switching, and gas sensing [40]. Their functional properties are highly influenced by parameters such as surface area, crystallinity, and the preparation method [41]. Several techniques are used to prepare V_2O_5 thin films, including chemical vapour deposition [42], the sol–gel method [43], and pulsed laser deposition (PLD) [44,45]. Among these, PLD is often reported as an inexpensive and low-energy process. It operates at low temperatures and offers advantages such as easy control over film thickness and composition through deposition parameters, as well as good reproducible stoichiometry from target to film, which is crucial for gas sensing [46]. This flexible and powerful method typically yields V_2O_5 thin films with various spherical grain sizes, averaging 50 nm, and surface roughness ranging from 9 to 20 nm [47]. Reports indicate that V_2O_5 thin films demonstrate a good response to oxidising gases such as NO_2, organic amines, ethanol, and ammonia at different temperatures (Table 2).

Table 2. Summary of V_2O_5 thin-film response towards different gases.

Thin-Film Material	Operation temperature (°C)	Targeted gas	Concentration (ppm)	Response*	Response time/Recovery time	Reference
Pristine V_2O_5	200	NO_2	100	41	20/150	[48,49]
Pristine V_2O_5	300	Ethanol	300	1.25	-5/8	[50]
Pristine V_2O_5	350	Hydrogen	5	23%	15/40	[51]
Pristine V_2O_5	200	Methane	50	23%	10 min	[51]
Pristine V_2O_5	RT	Xylene	5	27	80/50	[52,53]

 doi:10.20944/preprints202602.0309.v1

Pristine V_2O_5	200	Propane	50	0.05	15/30	[36,51]
V_2O_5-TiO_2	199.85-349.85	O_2	10 - 21%	-	-	[27]
V_2O_5-V_7O_{16}	620	NH_3	0.16-0.32	1.4	-	[54]

*Response calculated from $\frac{Rg-Ra}{Ra} * \mathbf{100}\%$ [49], and $\frac{Rg-Ra}{Ra} * \mathbf{100}\%$ [53].

Other studies have revealed that coupling V_2O_5 thin-film material with another composite material, such as V_7O_{16}, improves its response time. Table 2 shows that V_2O_5 coupled with V_7O_{16} results in improved response time compared to pure V_2O_5. Further, doping V_2O_5 thin films with titanium (Ti) leads to an n-p transition, which shows a good response towards hydrogen (5-300 ppm) as compared to the undoped n-type V_2O_5 thin [55]. In energy storage applications, doping V_2O_5 thin films with manganese (Mn) improves their cyclic stability [56]. For example, at a current density of $68mAg^{-1}$, Mn-doped V_2O_5 thin films have a discharge capacity of $283mAhg^{-1}$, which is significantly higher than pure V_2O_5 thin films $271mAhg^{-1}$ [57].

Other studies have shown that coupling V_2O_5 with another composite material, such as V_7O_{16}, improves its response time. As shown in Table 2, the V_2O_5/V_7O_{16} composite exhibits a faster response than pure V_2O_5. Furthermore, doping V_2O_5 thin films with titanium (Ti) induces an n-to-p transition, resulting in a good response to hydrogen (5–300 ppm) compared to undoped n-type V_2O_5 [55]. In energy storage applications, doping with manganese (Mn) improves cyclic stability [56]. For example, at a current density of 68 mA g^{-1}, Mn-doped V_2O_5 thin films achieve a discharge capacity of 283 mAh g^{-1}, significantly higher than the 271 mAh g^{-1} of pure V_2O_5 thin films [76].

2.3. V_2O_5 Nanorods

Vanadium pentoxide nanorods (Figure 4) exhibit nanoscale particles with a rod-like nanostructure. They are synthesised through versatile techniques, namely electrospinning, reverse-micelle, hydrothermal, DC magnetron deposition, etc. Their diameter and length are often measured between 150–200 nm and 1-10 μm [58] respectively, using the TEM. The morphology and size of these nanorods can be effectively manipulated by altering the calcination temperature during synthesis, with lower temperatures promoting the formation of smaller, more uniform nanorods [59]. V_2O_5 nanorods possess high reactivity and thermal stability, making them suitable for various applications, including catalysis, energy storage, fuel cells, and gas sensing. In particular, their large surface area and porous structure are conducive to efficient gas diffusion in the sensing layer, resulting in a quick response to the detection of various gases (Table 3) [60].

Vanadium pentoxide nanorods (Figure 4) are nanoscale particles with a rod-like morphology. They are synthesised through versatile techniques such as electrospinning, reverse-micelle, hydrothermal, and DC magnetron deposition. Their diameter and length typically range from 150–200 nm and 1–10 μm, respectively, as measured by TEM [78]. The morphology and size can be effectively tuned by altering the calcination temperature, with lower temperatures promoting smaller, more uniform nanorods [59]. V_2O_5 nanorods possess high reactivity and thermal stability, making them suitable for catalysis, energy storage, fuel cells, and gas sensing. Their large surface area and porous structure facilitate efficient gas diffusion in the sensing layer, leading to a quick response to various gases (Table 3) [60].

 doi:10.20944/preprints202602.0309.v1

Table 3. Summary of V_2O_5 nanorods response toward different gases at different temperatures and concentrations.

Material	Operation temperature (°C)	Targeted gas	Concentration (ppm)	Response*	Response time/Recovery time	Reference
Pristine V_2O_5	200	NO_2	100	24.2	13/140	[61]
p-type porous silicon (PS)/ V_2O	25	NO_2	0.25	7.4	2/6	[28,62]
Pd-V_2O_5	200	NO_2	100	75	22/126	[48,53]
Pristine V_2O_5	RT	Ethanol	100	3.7%	-	[58]
Pristine V_2O_5	RT	Ammonia	500	1.8%	23/15	[39,58]
Te-V_2O_5	RT	Ethanol	500	1.8%	3.5	[53,63]

*Response calculated from and $\frac{\Delta R}{Ra} * \mathbf{100\%}$ [62]; Response from $\frac{Rg-Ra}{Ra} * \mathbf{100\%}$ [53] and Responsivity from $\frac{Rg-Ra}{Ra} * \mathbf{100\%}$ [39].

Doping the surface of V_2O_5 nanorods with Tellurium (Te) through a hydrothermal method has been reported to be an effective method to enhance its sensitivity. Te is reported to have a nanorod-like structure, and doping it into V_2O_5 nanorods tends to produce a greater number of reactive sites and also increase the surface-to-volume ratio, which improves the sensitivity of the sensor [63]. Other reports have also revealed that doping the V_2O_5 nanorod's surface with palladium (Pd) noble metal tends to improve the selectivity of the sensor and decrease the response-recovery times. Pds act as a catalyst and agitate the surface interaction between the sensing layer and the targeted gas [48]. Pd-sensitised V_2O_5 sensor has high porosity nanostructure and greater surface activities. The absorption of the gas takes place on the Pd and then spills over into V_2O_5.

Doping V_2O_5 nanorods with tellurium (Te) via a hydrothermal method has been reported to enhance sensitivity. Te itself has a nanorod-like structure, and its incorporation is believed to increase the number of reactive sites and the surface-to-volume ratio, thereby improving sensor sensitivity [63]. Other reports indicate that doping with palladium (Pd) improves selectivity and reduces response and recovery times. Pd acts as a catalyst, promoting surface interactions between the sensing layer and the target gas [48]. Pd-sensitised V_2O_5 sensors exhibit high porosity and greater surface activity, where gas absorption occurs first on Pd before spilling over to V_2O_5.

The Pd-sensitised V_2O_5 nanorod sensor exhibits a different sensing mechanism from the pristine V_2O_5 nanorod sensor, which follows the general mechanism of an n-type metal-semiconductor. Upon exposure of the Pd-sensitised V_2O_5 nanorods sensor to atmospheric air. The dissociation of the oxygen molecule takes place in the Pd particle, and the adsorbed (O_2^-, O^-, and O) species diffuses into the surface of the V_2O_5 nanorods, resulting in a space charge region with a high potential barrier [64]. This leads to high resistance on the surface of the nanorods. When the Pd-sensitised V_2O_5 nanorods sensor is then set to a reducing gas atmosphere such as ethanol, the catalytic effect of Pd facilitates

 doi:10.20944/preprints202602.0309.v1

the reaction between the surface of the material and adsorbed species, which results in a release of an electron back to the conduction band [61]. The potential barrier reduces, resulting in a decrease in resistance and an increase in conductance. [51,65,66].

The sensing mechanism of Pd-sensitised V_2O_5 nanorods differs from that of pristine V_2O_5, which follows the general n-type metal oxide mechanism. When exposed to air, oxygen molecules dissociate on Pd particles, and the resulting adsorbed species (O_2^-, O^-, O) diffuse onto the V_2O_5 nanorod surface, creating a space-charge region with a high potential barrier [64]. This leads to high surface resistance. Upon exposure to a reducing gas like ethanol, the catalytic effect of Pd facilitates a reaction between the gas and adsorbed oxygen, releasing electrons back into the conduction band [61]. This reduces the potential barrier, decreasing resistance and increasing conductance [51,65,66].

2.4. V_2O_5 Nanofibers

Nanofibers are nanoparticle fibres that are often used in energy storage, drug delivery, biometric materials, and gas sensors due to their high surface-to-volume ratio [67,68]. V_2O_5 nanofibers are distinguished from other nanostructures (nanowires, nanoribbons, nanoneedles, nanorods, and nanotubes) by their regular structure (1.5 nm × 10 nm cross-section), [69,70]. These nanofibers are synthesised by combined methods (electrospinning and the sol-gel) which have proven to produce small-diameter fibers that require no expensive purification [71,72]. Both electrospinning and sol-gel methods are well-known for their low cost, and combining the two results in long, continuous, uniform nanofibers with a very significant surface area and reduced diameter [73]. V_2O_5 nanofibers are often prepared as an n-type semiconductor with an electronic conductivity of 0.5 cm^{-1} at room temperature, which makes it an ideal material for novel devices that can operate at room temperature [74]. These unique electronic conductivity properties allow V_2O_5 nanofibers to be used as an ideal gas sensor material and have shown a good response time when detecting different gases. (Table 4). The addition (doping) of a small amount of silver (Ag) to the surface of V_2O_5 nanofibers increases the selectivity and sensitivity of the material tremendously. When V_2O_5 nanofiber is doped with Ag (Ag-V_2O_5), the width of the nanofiber formed ranges from 8 nm to 15 nm, which is similar to a pure V_2O_5 nanofiber (width of ~10 nm) [70].

Nanofibers are nanoparticle fibres widely used in energy storage, drug delivery, biometric materials, and gas sensors due to their high surface-to-volume ratio [67,68]. V_2O_5 nanofibers are distinguished from other nanostructures (nanowires, nanoribbons, nanoneedles, nanorods, and nanotubes) by their regular structure, typically with a cross-section around 1.5 nm × 10 nm [69,70]. They are often synthesised by combined methods such as electrospinning and sol–gel, which produce small-diameter fibers without requiring expensive purification [71,72]. Both techniques are low-cost, and their combination yields long, continuous, uniform nanofibers with a high surface area and reduced diameter [73]. V_2O_5 nanofibers are typically n-type semiconductors with an electronic conductivity of ~0.5 Ω^{-1} cm^{-1} at room temperature, making them suitable for novel room-temperature devices [74]. These conductive properties make V_2O_5 nanofibers an ideal gas sensing material, and they have shown good response times to various gases (Table 4). Doping with a small amount of silver (Ag) significantly increases both selectivity and sensitivity. Ag-doped V_2O_5 nanofibers have a width ranging from 8 to 15 nm, similar to that of pure V_2O_5 nanofibers (~10 nm) [70].

Table 4. Summary of V_2O_5 nanofibers response toward different gases.

Nanofibers Material	Operation temperature (°C)	Targeted gas	Concentration (ppm)	Response *	Response time/Recovery time	Reference
Pristine V_2O_5	RT	1-butylamine	0.03	42	250/700	[53]

 doi:10.20944/preprints202602.0309.v1

Pristine V_2O_5	RT	Xylene	5	1.7	-	[52]
Pristine V_2O_5	150	Ammonia	0.1	11	50/350	[39,75]
SnO_2- V_2O_5	325	Benzene	25	6.35	-	[76]

*Response calculated from $\frac{Rg-Ra}{Ra} * 100\%$ [53] and $\frac{Rg-Ra}{Ra} * 100\%$ [39].

2.5. V_2O_5 Nanoflowers

Vanadium pentoxide nanoflowers are nanostructured particles that resemble a flower pattern [77]. They are made up of ultrathin nanowires and nanoribbons. The large surface-to-volume ratio of ultrathin particles provides a strong surface effect, which is very beneficial for gas adsorption [78]. The space between the lateral dimensions of the sheets in the nanoflower structure enhances the surface area, providing additional reactive sites for the target chemical [79]. Flower-like V_2O_5 hierarchical structure exhibits unusual p-type semiconductor features below 100°C which is the result of the ultrathin structure of the nanowire and nanoribbon [80]. V_2O_5 nanoflower-like structures can be synthesised using various methods such as hydrothermal process [81], water bath method [82], and electrochemical process [83]. The diameter of each petal in the nanoflower usually consists of a thickness less than 100 nm, and the diameter ranges between 400–700 nm [84]. V_2O_5 nanoflowers are heavily explored in the gas sensing application because of their high surface-to-volume ratio, higher surface activity, and high thermal stability [85]. Different studies have reported on using V_2O_5 nanoflowers for the detection of different gases. (Table 5).

Vanadium pentoxide nanoflowers are nanostructured particles with a flower-like pattern, composed of ultrathin nanowires and nanoribbons [77]. The large surface-to-volume ratio of these ultrathin components provides a strong surface effect, which is highly beneficial for gas adsorption [78]. The spacing between the sheets in the nanoflower structure further increases the surface area, providing additional reactive sites for target chemicals [79]. Flower-like V_2O_5 hierarchical structures exhibit unusual p-type semiconductor behaviour below 100 °C, a result of their ultrathin nanowire and nanoribbon building blocks [80]. They can be synthesised via various methods, including hydrothermal processing [81], the water bath method [82], and electrochemical processes [83]. Each petal typically has a thickness below 100 nm and a diameter between 400–700 nm [84]. V_2O_5 nanoflowers are extensively explored for gas sensing due to their high surface-to-volume ratio, surface activity, and thermal stability [85]. Various studies have reported their use in detecting different gases (Table 5).

Table 5. Summary of V_2O_5 nanoflower response toward different gases.

Nanofibers Material	**Operation temperature (°C)**	**Targeted gas**	**Concentration (ppm)**	**Response ***	**Response time/Recovery time**	**Reference**
Pristine V_2O_5	250	Ammonia	100	4.5	-	[86]
Pristine V_2O_5	250	Ethanol	5-1000	5.3	-	[87]
Pristine V_2O_5	300	Xylene	100	2.2	-	[88]

 doi:10.20944/preprints202602.0309.v1

SnO_2- V_2O_5	140	Butylamine	100	2.6	9/49	[89]

*Response calculated $\frac{Rg-Ra}{Ra} * 100\%$ [39].

The gas sensor based on a nanoflower V_2O_5 has demonstrated a significantly quicker response towards the detection of ethanol and methane gas at different concentration levels compared to other morphologies, including honeycomb-like and nano-chain, especially [90]. Moreover, this material has also demonstrated an increased sensitivity towards ethanol gas at a concentration of 1.37–25 ppm, which is substantially lower than the breath analyser limit (200 ppm) at room temperature [91]. The superior performance of nanoflower is highly attributed to its porous and high crystalline nature [91].

Gas sensors based on V_2O_5 nanoflowers demonstrate a significantly faster response to ethanol and methane at various concentration levels compared to other morphologies such as honeycomb-like and nanochain structures [90]. Moreover, they exhibit increased sensitivity to ethanol at concentrations of 1.37–25 ppm, substantially below the typical breath analyser limit of 200 ppm, and can operate at room temperature [91]. This superior performance is attributed to their porous and highly crystalline nature [91].

2.6. V_2O_5 nanowires

Nanowires are often referred to as one-dimensional (1D) or quasi-materials that resemble a wire. These materials are synthesised by a variety of techniques, including hydrothermal, chemical vapour deposition (CVD), sol-gel, and electrospinning [92,93]. Electrospinning is the most commonly used technique due to its ability to produce nanowires with high porosity and high surface area. The average diameter of each nanowire synthesised by electrospinning is found to be 200-250 nm [94]. Over the years, V_2O_5 nanowires have been used in a wide range of applications such as electrodes in supercapacitors, components in lithium-ion batteries, and catalysis in organic synthesis. V_2O_5 nanowires have also been widely used in electrochemical sensors as a sensing material due to their unique properties, such as a large surface-to-volume ratio, superior stability owing to the high degree of crystallinity, and dimensions comparable to the extension of the surface charge region [95,96]. V_2O_5 nanowires have shown good response towards different gases at different concentrations and temperatures.

Nanowires are one-dimensional (1D) or quasi-1D materials with a wire-like morphology. They are synthesised by various techniques, including hydrothermal, chemical vapour deposition (CVD), sol–gel, and electrospinning [92,93]. Electrospinning is the most common due to its ability to produce nanowires with high porosity and surface area; the average diameter of electrospun nanowires is typically 200–250 nm [94]. V_2O_5 nanowires have been used in supercapacitor electrodes, lithium-ion battery components, and catalysis in organic synthesis. They are also widely used in electrochemical sensors due to their unique properties: a large surface-to-volume ratio, superior stability from high crystallinity, and dimensions comparable to the extent of the surface charge region [95,96]. V_2O_5 nanowires show good responses to various gases at different concentrations and temperatures.

Table 6. Summary of V_2O_5 nanowire response toward different gases.

Nanowire Material	Operation temperature (°C)	Targeted gas	Concentration (ppm)	Response *	Response time/Recovery time	Reference
Pristine V_2O_5	330	Ethanol	9.09-1000	9	-	[97]

 doi:10.20944/preprints202602.0309.v1

Pristine V_2O_5	200	NO_2	20	41%	20/150	[98]
Pristine V_2O_5	330	Ammonia	1000	1.8	-	[99]
Pristine V_2O_5	-RT	He	0-17.6	5%	-	[100]
CuO/V_2O_5	220	Hydrogen Sulphide	23	31.86	-	[100]
SnO_2-V_2O_5	RT	Ethanol	100	14	-	[101]

Response calculated $\frac{Rg-Ra}{Ra} * 100\%$.

However, studies have indicated that materials of nanowire structure are not commonly available due to the fact that they show non-uniform growth, poor control over density and distribution, reproducible contact between nanowires and electrodes, and sensor geometry [102]. Modification of the V_2O_5 nanowire surface via decorating with other oxides such as tin oxide (SnO_2) and copper oxide (CuO) (Table 6) has been reported to be an effective method to enhance its response time and sensitivity towards the detection of different gases. Previous reports have indicated that SnO_2-decorated V_2O_5 exhibits a heterojunction interface structure that possesses a more enhanced response toward ethanol gas compared to pristine V_2O_5. Further, using a p-type CuO (work function of 5.3 eV) to decorate n-type V_2O_5 (work function of 4.7 eV) has been found to create a p-n junction structure with enhanced sensitivity towards acetone [103].

However, nanowire-based materials face challenges, including non-uniform growth, poor control over density and distribution, difficulty in achieving reproducible contact between nanowires and electrodes, and constraints in sensor geometry [102]. Modifying the V_2O_5 nanowire surface by decorating it with other oxides, such as tin oxide (SnO_2) and copper oxide (CuO), has been reported as an effective method to enhance response time and sensitivity (Table 6). Previous reports indicate that SnO_2-decorated V_2O_5 forms a heterojunction interface with an enhanced response to ethanol compared to pristine V_2O_5. Furthermore, decorating n-type V_2O_5 (work function ~4.7 eV) with p-type CuO (work function ~5.3 eV) creates a p–n junction structure with enhanced sensitivity to acetone [103].

2.7. V_2O_5 Nanotubes

Vanadium pentoxide (V_2O_5) nanotubes are nanoparticles with a tubular morphology composed of three distinct regions: inner surface, outer surface, and tube ends [104–106]. These nanotubes are often synthesised by the sol-gel technique followed by hydrothermal [107,108]. Their inner and outer diameters usually range between 20-40 nm and 80-100 nm, respectively [104,109]. V_2O_5 nanotubes have been found to be efficient for electrochemical and catalytic applications due to their large surface area and various ionic transport channels. Further, these nanotubes have been identified as viable materials for gas sensing applications, demonstrating good response towards the detection of different gases at different temperatures (Table 7) [104,110,111].

Vanadium pentoxide (V_2O_5) nanotubes are nanoparticles with a tubular morphology composed of three distinct regions: the inner surface, outer surface, and tube ends [104–106]. They are typically synthesised by a sol–gel technique followed by a hydrothermal step [107,108]. Their inner and outer diameters usually range from 20–40 nm and 80–100 nm, respectively [104,109]. V_2O_5 nanotubes are

 doi:10.20944/preprints202602.0309.v1

efficient for electrochemical and catalytic applications due to their large surface area and multiple ionic transport channels. They are also promising for gas sensing, demonstrating good responses to various gases at different temperatures (Table 7) [104,110,111].

Table 7. Summary of V_2O_5 nanotube response toward different gases.

Nanotube Material	Operation temperature (°C)	Targeted gas	Concentration (ppm)	Response*	Response time/Recovery time (s)	Reference
Pristine V_2O_5	330	Ethanol	100	2.6	5/5	[112]
V_2O_5/Au	200	Ethanol	100	2.7	7/5	[112]
V_2O_5/Fe_2O_3	330	Ethanol	100	1.3	15/20	[113]

The surface doping of V_2O_5 nanotube with transition metals has been reported to effectively enhance their electric and magnetic properties [114]. The openings at the endpoints of the nanotubes are especially suitable for introducing noble metals, and the intercalation of Au into V_2O_5 nanotubes has been reported to provide more active sites for gas adsorption and allow good sensitivity [112].

Surface doping of V_2O_5 nanotubes with transition metals effectively enhances their electrical and magnetic properties [114]. The open ends of the nanotubes are particularly suitable for introducing noble metals. For example, intercalating gold (Au) into V_2O_5 nanotubes provides more active sites for gas adsorption and improves sensitivity [112].

The sensing mechanism of a V_2O_5 nanotube sensor follows the general sensing mechanism of an n-type semiconductor and can be explained by the space charge region model [115]. However, a different sensing mechanism is observed for a doped Au/V_2O_5 nanotube sensor. Upon exposure to air, electrons are transferred from the surface of the V_2O_5 nanotube to the Au particle due to the Schottky junction between the metal and the semiconductor. [50]. Au acts as a catalytic activator in promoting the dissociation of an oxygen atom into O_2^-, O^-, and O-adsorbed species, which are transported into the nanotube surface [116]. When the Au/V_2O_5 nanotube sensor is subjected to ethanol gas, the gas molecules react with the adsorbed oxygen species, and the captured electrons are released into the V_2O_5 conduction band, thereby decreasing the resistance [117].

The sensing mechanism of a pristine V_2O_5 nanotube sensor follows the general n-type semiconductor model, explained by the space-charge region model [115]. However, a different mechanism operates for Au-doped V_2O_5 nanotubes. Upon air exposure, electrons transfer from the V_2O_5 nanotube surface to Au particles due to the Schottky junction between the metal and semiconductor [50]. Au acts as a catalytic activator, promoting the dissociation of oxygen into O_2^-, O^-, and O adsorbed species, which then migrate to the nanotube surface [116]. When exposed to ethanol, the gas molecules react with these adsorbed oxygen species, releasing captured electrons into the V_2O_5 conduction band and thereby decreasing resistance [117].

3. Density Functional Theory (DFT) Perspective

This review article has so far intensively discussed the impact of hierarchical structures towards gas sensing using the experimental approach. However, to explore the full extent of the analyses, we need to consider the quantum mechanical aspect based on density functional theory (DFT) calculations. Previous studies have used DFT to investigate different properties of hierarchical structures, including band structure, density of states, elastic constants, absorption energy, and optical properties. For example, first principles calculations have been used to explore the energetics, electronic and geometric structures of zinc sulphide (ZnS) nanotubes, nanorods, nanosheets, and

 doi:10.20944/preprints202602.0309.v1

nanowires based on their thickness or diameter, and its effect on the band gap. Results revealed that ZnS nanowires and double-wired nanotube with higher thickness diameter were the most energetically favoured hierarchical structures, compared to single-wired ZnS nanotubes [118]. The band gap size of these hierarchical structures was found to decrease with an increase in diameter, resulting in high conductivity. Other works also used DFT to estimate the band gap of copper oxide (CuO) thin films, which was found to be 1.66 eV, in agreement with experimental results [119]. In addition, this tool has also been used to gain an atomic-level understanding of how hierarchical structures interact with adsorbate gas molecules. It was observed that ZnS nanotubes showed a high response to ammonia and phosphine, due to the structural orientation of the gas molecules. The sensitivity of a tube was found to be more favourable towards the chemisorption mode [120].

This review has thus far intensively discussed the impact of hierarchical structures on gas sensing from an experimental perspective. To explore the full extent of the analysis, we must also consider the quantum mechanical aspect based on density functional theory (DFT) calculations. Previous studies have used DFT to investigate various properties of hierarchical structures, including band structure, density of states, elastic constants, adsorption energy, and optical properties. For example, first-principles calculations have been employed to explore the energetics and the electronic and geometric structures of zinc sulphide (ZnS) nanotubes, nanorods, nanosheets, and nanowires as a function of their thickness or diameter, and the consequent effect on band gap. Results revealed that ZnS nanowires and double-walled nanotubes with larger diameters were the most energetically favorable hierarchical structures compared to single-walled ZnS nanotubes [118]. The band gap of these structures was found to decrease with increasing diameter, resulting in higher conductivity. DFT has also been used to estimate the band gap of copper oxide (CuO) thin films, yielding a value of 1.66 eV which agrees with experimental results [119]. Furthermore, this computational tool provides an atomic-level understanding of how hierarchical structures interact with adsorbate gas molecules. For instance, ZnS nanotubes showed a high response to ammonia and phosphine due to the structural orientation of the gas molecules, with sensitivity found to be more favorable toward the chemisorption mode [120].

Other studies have also employed the DFT to simulate stable surfaces of various hierarchical structures. Reports have demonstrated that (010) V_2O_5 nanobelts have a good response to the adsorption of ethanol gas. Atomic Mulliken population analysis revealed a transfer of 0.18e electrons from the ethanol gas into the nanobelt's conduction band, resulting in increased conductivity. Furthermore, the reaction's enthalpy change was reported to be −2.84 eV, signifying an exothermic reaction, which is in agreement with experimental findings [121]. Similar effects were observed when (001) nanorods were loaded with NH_3 molecules, wherein the band gap of the nanorods reduced with increasing loading of NH_3 molecules, indicating electron transfer from NH_3 to the nanorod and corresponding shift of the Fermi level towards the conduction band [122].

Other studies have employed DFT to simulate stable surfaces of various hierarchical structures. Reports demonstrate that the (010) surface of V_2O_5 nanobelts exhibits a strong response to ethanol adsorption. Atomic Mulliken population analysis revealed a charge transfer of 0.18 e from ethanol to the nanobelt's conduction band, increasing conductivity. The reaction enthalpy change was reported to be −2.84 eV, signifying an exothermic process consistent with experimental findings [121]. A similar effect was observed when (001) nanorods were exposed to NH_3 molecules; the band gap decreased with increasing NH_3 loading, indicating electron transfer from NH_3 to the nanorod and a corresponding shift of the Fermi level toward the conduction band [122].

Further, DFT has been found to play a significant role in determining the type of transition metal dopants likely to improve the adsorption energies and electronic properties of materials. Reports have shown that doping carbon nanotubes (CNT) with Sc, Ti, V and Cr can drastically alter the electronic properties, resulting in enhanced NH_3, PH_3 and AsH_3 adsorption energies. It was reported that doping CNT with Cr shows a band gap of 0.707 eV, resulting in higher adsorption energy to NH_3 in comparison to the other dopants [123]. The natural bond orbital that indicates the charge transfer of NH_3 to the CNT was found to be 0.195e, indicating a strong covalent bond [123]. Additionally, it

 doi:10.20944/preprints202602.0309.v1

has also been reported that intercalation of metal atoms such as Rhodium (Rh) into (001) phase of V_2O_5 reduces the band gap of the material from 2.2 eV to 0.3 eV [159]. Rh becomes the centre of attraction when the material is exposed to some gases such as CO, PH_3, and H_2S. In the case of CO exposure, the most stable adsorption is when the C atom is adsorbed on Rh, yielding an energy of -296 meV as compared to the pristine V_2O_5, which gives the adsorption energy of -137 meV. However, polar molecules such as SO_2, and CO_2 prefer to adsorb on the V atom, which is supported by charge contour plots analysis that shows polar molecules bond via the oxygen atom to the zone near the V and bridging O_2 atom [123]. Thus, the pre-adsorption of Rh on the surface of (001) V_2O_5 results in a weaker interaction between (001) V_2O_5 and CO_2 [123].

DFT also plays a significant role in screening transition metal dopants to improve adsorption energies and electronic properties. For example, doping carbon nanotubes (CNTs) with Sc, Ti, V, and Cr can drastically alter electronic properties, enhancing the adsorption energies for NH_3, PH_3, and AsH_3. Specifically, Cr-doped CNTs exhibit a band gap of 0.707 eV and higher adsorption energy for NH_3 compared to other dopants [146]. The natural bond orbital analysis indicated a charge transfer of 0.195 e from NH_3 to the CNT, suggesting a strong covalent interaction [123]. Additionally, intercalating metal atoms such as rhodium (Rh) into the (001) phase of V_2O_5 reduces the band gap from 2.2 eV to 0.3 eV [159]. Rh acts as an active centre when the material is exposed to gases such as CO, PH_3, and H_2S. For CO exposure, the most stable configuration involves adsorption of the C atom on Rh, with an adsorption energy of −296 meV, compared to −137 meV for pristine V_2O_5. In contrast, polar molecules such as SO_2 and CO_2 prefer to adsorb on V atoms, supported by charge contour plots showing that these molecules bond via an oxygen atom near the V and bridging O atoms [123]. Thus, pre-adsorption of Rh on the (001) V_2O_5 surface weakens the interaction with CO_2 [123].

This current study employed DFT to investigate the effect of doping vanadium pentoxide (V_2O_5) with transition metals including tungsten (W), copper (Cu), manganese (Mn), tin (Sn), and silver (Ag) to enhance its adsorption energy towards nitrogen dioxide (NO_2). Incorporating foreign metals in the surface of V_2O_5 has been previously reported to improve the electromechical properties of the material. For instance, doping V_2O_5 with Ag and Cu have shown to improve the electric conductivity properties by two order magnitude. This dopant has been believed reduce the oxidation of vanadium ion state from V^{5+} to V^{4+} resulting in oxygen vacancies in the material which are more beneficial for gas adsorption, especially to reducing gases. As such in this present work we intensively reviewed the sensing performances of nano layered hierarchical V_2O_5 structures and comprehensively study the gas molecule adsorption properties of pristine and doped V_2O_5 from ab initio approach. The different transition metals were incorporated using the substitution methods.

In the current study, DFT was employed to investigate the effect of doping vanadium pentoxide (V_2O_5) with transition metals—tungsten (W), copper (Cu), manganese (Mn), tin (Sn), and silver (Ag)—to enhance its adsorption energy toward nitrogen dioxide (NO_2). Incorporating foreign metals into V_2O_5 has been previously reported to improve its electrochemical properties. For instance, doping with Ag and Cu can improve electrical conductivity by two orders of magnitude. These dopants are believed to reduce the oxidation state of vanadium from V^{5+} to V^{4+}, creating oxygen vacancies that are beneficial for gas adsorption, particularly for reducing gases. Therefore, this work comprehensively reviews the sensing performance of nano-layered hierarchical V_2O_5 structures and provides a detailed *ab initio* study of gas molecule adsorption on pristine and doped V_2O_5. The different transition metals were incorporated using substitutional doping methods.

3.1. Density Functional Theory Study of Transition-Metal-Doped V_2O_5 for Enhanced Adsorption of NO_2

Bulk alpha vanadium pentoxide (α-V_2O_5) is classified as an orthorhombic crystal structure with a space group 59 (Pmmn). The basis (Figure 9a) consists of identical vanadium atoms and three nonequivalent oxygen atoms, namely: vanadyl oxygen (O_v), bridging oxygen (O_b), and Chain oxygen (O_c). This structure is composed of a distorted octahedra with one central vanadium atom bonded to six oxygen atoms (VO_6). (See Figure 9b) Each VO_6 is linked together at the edges by the chain (O_c) and at the corners by the bridging (O_b). The vanadyl (V=O_v) is double-bonded to a single vanadium atom,

 doi:10.20944/preprints202602.0309.v1

with a bond distance of 1.610 Å, while the bridging (V-O_b) is bonded to two adjacent vanadium atoms with a bond distance of 1.806 Å, and chain (V-O_c) atoms are bonded to three vanadium atoms with a bond distance of 1.88 Å, respectively.

Bulk alpha vanadium pentoxide (α-V_2O_5) has an orthorhombic crystal structure with space group *Pmmn* (No. 59). Its unit cell (Figure 9a) contains identical vanadium atoms and three nonequivalent oxygen atoms: vanadyl oxygen (O_v), bridging oxygen (O_b), and chain oxygen (O_c). The structure consists of distorted VO_6 octahedra (Figure 9b), each with a central vanadium atom bonded to six oxygen atoms. Adjacent VO_6 units are linked at edges by chain oxygen (O_c) and at corners by bridging oxygen (O_b). The vanadyl oxygen (V=O_v) is double-bonded to a single vanadium atom with a bond distance of 1.610 Å, while the bridging oxygen (V–O_b) bonds to two adjacent vanadium atoms at 1.806 Å, and the chain oxygen (V–O_c) bonds to three vanadium atoms at 1.88 Å.

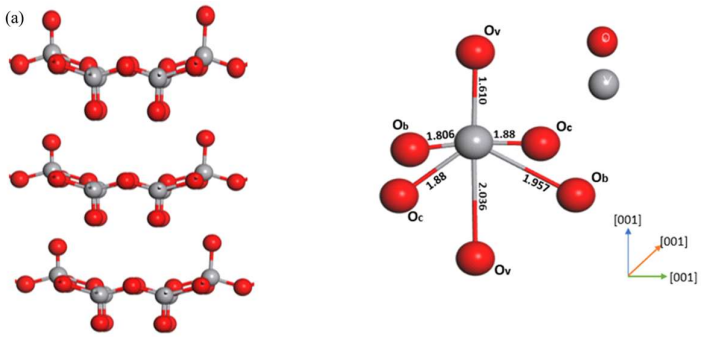

Figure 2. (a) Crystal structure of V_2O_5 and (b) Coordination of a vanadium and oxygen atom in V_2O_5. The red balls represent oxygen, and the grey represents the vanadium atom.

In order to determine the ground state properties of V_2O_5, Full geometry optimisation of the V_2O_5 unit cell was performed using plane pseudopotential wave density functional theory calculations, as implemented in the CASTEP. Vanderbilt ultrasoft pseudopotentials were used to describe the valence-core interactions, while the Perdew-Burke-Ernzerhof generalized gradient approximation functional was used to approximate the electronic exchange correlation effects. A plane wave cut-off of 1000 eV and a k-point sampling of 4×14×11 was found to be sufficient to converge the bulk V_2O_5. The optimised lattice constants and the bond distances were compared with the experiment and literature as summarised in Table 8. Our calculated lattice parameters and bond lengths are in good agreement with experimental and literature values.

To determine the ground-state properties of V_2O_5, full geometry optimisation of the unit cell was performed using plane-wave pseudopotential density functional theory as implemented in CASTEP. Vanderbilt ultrasoft pseudopotentials described the valence–core interactions, and the Perdew–Burke–Ernzerhof generalized gradient approximation functional was used for the exchange–correlation effects. A plane-wave cut-off energy of 1000 eV and a *k*-point mesh of 4 × 14 × 11 were sufficient to converge the bulk V_2O_5 properties. The optimised lattice constants and bond distances were compared with experimental and literature values, as summarised in Table 8. Our calculated parameters show good agreement with previous data.

 doi:10.20944/preprints202602.0309.v1

Table 8. Comparison of the optimised lattice parameters and bond lengths, comparison with experiment and literature (Calculated).

	This work (GGA)	Experiment [124]	Literature (Calculated) [125]
Lattice parameters (Å)			
a	3.62	3.56	3.56
b	4.79	4.37	4.37
c	11.55	11.51	11.51
Bond length (Å)			
vanadyl oxygen (O_v)	1.61	1.54	1.61
bridge oxygen (O_b)	1.81	1.88	1.78
chain oxygen (O_c)	2.04	2.02	2.02

3.2. Adsorption of NO_2 Molecule V_2O_5 (011) Surface

The adsorption of NO_2 molecule in this study was modeled using a V_2O_5 (011) surface supercell. The (011) plane is proven to be the most thermodynamically stable compared to other V_2O_5 such as (100), (200), and (400). V_2O_5 surface was constructed by cleaving the optimised bulk V_2O_5 in the (011) direction and building a 2×2 supercell slab of four repeat units. A vacuum space of 20 Å was allowed to ensure negligible interaction with image slabs. Adsorption of the NO_2 molecule was performed for both the clean and transition metals (Cu, Mn, Ag, Sn) doped V_2O_5 surfaces, with the metal atom substituting the atom located on the top layer of the surface slab, as shown in Figure 3. The adsorption energies in each case were calculated using the equation

The adsorption of NO_2 was modeled on a V_2O_5 (011) surface supercell, chosen for its thermodynamic stability relative to other surfaces such as (100), (200), and (400) [reference]. The surface was constructed by cleaving the optimised bulk V_2O_5 along the (011) direction to create a 2 × 2 supercell slab of four repeat units. A vacuum space of 20 Å was added to avoid interactions between periodic images. Adsorption was studied on both pristine and transition-metal-doped (Cu, Mn, Ag, Sn) V_2O_5 surfaces, with the dopant atom substituting a top-layer vanadium atom (Figure 3). The adsorption energy (E_a) for each case was calculated using the equation:

$$\boldsymbol{E_a = E_{system} - (E_{surface} + E_{adsorbate})}$$

where $\boldsymbol{E_{system}}$ is the total energy of the optimised (undoped or doped)V_2O_5 adsorbed surfaces whereas $\boldsymbol{E_{surface}}$ and $\boldsymbol{E_{adsorbate}}$ denote the total energy of the doped and clean surfaces and energy of the NO_2 molecule, respectively. A negative value of $\boldsymbol{E_a}$ indicates that the process is exothermic, whereas a positive value indicates an endothermic process.

Where $\boldsymbol{E_{system}}$ is the total energy of the optimised (doped or undoped) V_2O_5 surface with adsorbed NO_2, $\boldsymbol{E_{surface}}$ is the total energy of the clean (doped or undoped) surface, and $\boldsymbol{E_{adsorbate}}$ is the energy of an isolated NO_2 molecule. A negative $\boldsymbol{E_a}$ indicates an exothermic process, while a positive value indicates an endothermic one.

Figure 4 presents the adsorption energy of NO_2 on clean and transition metal-doped V_2O_5 (011) surface calculated for different numbers of NO_2 molecules. It is seen that all the calculated adsorption energies are negative, indicating that the reaction between the surface and the adsorbate occurs

 doi:10.20944/preprints202602.0309.v1

spontaneously. Increasing the load of NO_2 molecules leads to a reduction in the adsorption energy in both the clean and doped V_2O_5 surface, but while remaining in the negative regime, indicating a possibility of sensing application over a wide range of concentrations. Clearly, Ag-doped V_2O_5 presents the most negative adsorption energy as compared to the clean and the other dopants (see Figure 5). However, at concentrations beyond four NO_2 molecules, the adsorption energy of the clean surface becomes more negative, indicating that Ag doping may play a critical role in increasing the sensing effectiveness of V_2O_5 at low concentrations of NO_2 molecules.

Figure 4 presents the adsorption energies of NO_2 on pristine and transition-metal-doped V_2O_5 (011) surfaces for varying numbers of NO_2 molecules. All calculated adsorption energies are negative, indicating spontaneous adsorption. Increasing the NO_2 load reduces the adsorption energy (though remaining negative) for both pristine and doped surfaces, suggesting potential for sensing over a wide concentration range. Notably, Ag-doped V_2O_5 exhibits the most negative adsorption energy compared to the pristine surface and other dopants (see Figure 5). However, beyond four NO_2 molecules, the adsorption energy of the pristine surface becomes more negative, indicating that Ag doping may be particularly effective in enhancing V_2O_5 sensitivity at low NO_2 concentrations.

Similar results have been reported experimentally when comparing $Ag_{0.35}$ V_2O_5 with undoped V_2O_5. The $Ag_{0.35}$ V_2O_5 material tends to show high sensitivity and selectivity toward different gases (including ammonia, acetone, and amines) at 100 ppm concentration. This is due to the decrease in electronegativity of vanadium (V) in $Ag_{0.35}$ V_2O_5, which results in the high absorbing site [126]. The other dopants, such as Cu, Ag, and Mn, have also enhanced the structural stability of V_2O_5 at higher concentrations of NO_2 molecules. The graph tends to increase beyond the saturation phase (four NO_2 molecules) on the undoped surface.

Similar results have been reported experimentally for $Ag_{0.35}V_2O_5$, which shows higher sensitivity and selectivity toward gases such as ammonia, acetone, and amines at 100 ppm concentration. This is attributed to decreased electronegativity of vanadium in $Ag_{0.35}V_2O_5$, leading to more favorable adsorption sites [126]. Other dopants (Cu, Mn, Sn) also enhance the structural stability of V_2O_5 at higher NO_2 concentrations, as the adsorption energy trend rises beyond the saturation point observed for the undoped surface.

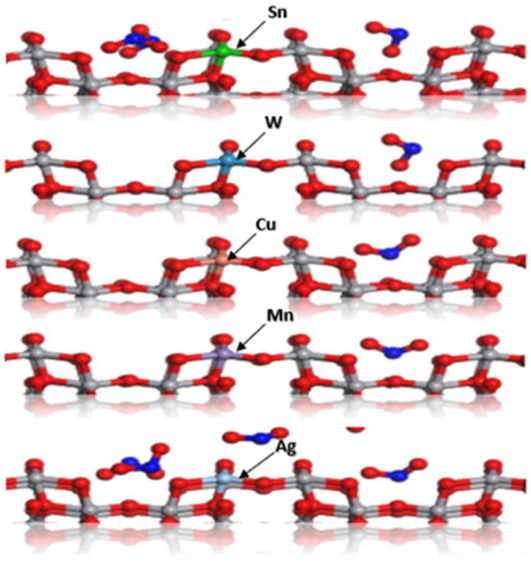

Figure 3. Geometry-optimised V_2O_5 supercell doped with Sn, W, Cu, Mn, and Ag.

 doi:10.20944/preprints202602.0309.v1

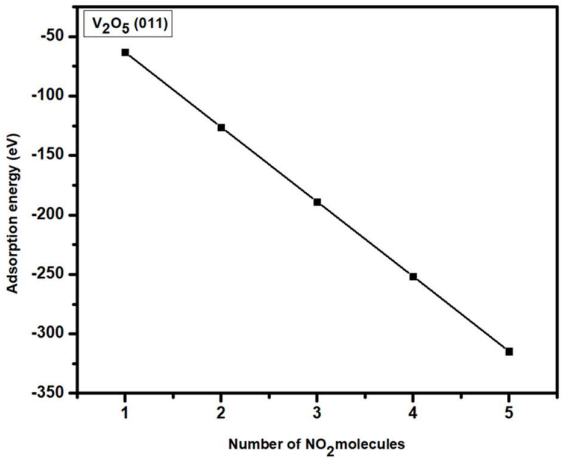

Figure 4. Adsorption energy vs number of NO_2 molecules.

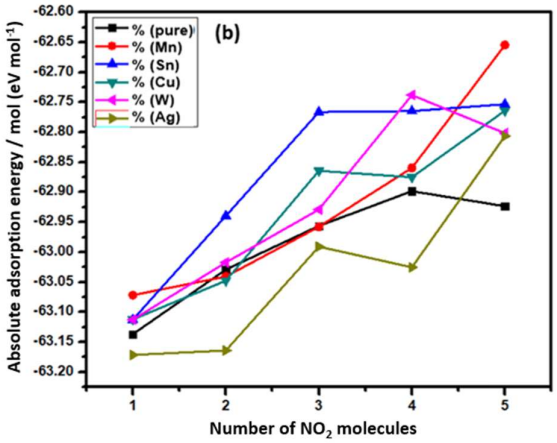

Figure 5. Adsorption energy of per molecule of NO_2 on V_2O_5 (011) clean and transition metal doped surfaces calculated for different number of NO_2 molecules.

4. Conclusions

This paper presents a review of hierarchical nano-layered V_2O_5 structures for application in gas sensing and gas sensing technology. Various morphologies and atomic structures, ranging from nanowires to nano thin films, were reviewed in terms of their gas detection capabilities, such as target gas, concentration, response, and recovery times were discussed. The work also successfully analysed the temperature of detection of those nanorod structures that have been studied more at room temperature, since these are more likely to be energy efficient in practical applications. It was further found that most structures and morphologies in many studies explored ethanol and NO_2 as preferred gases for detection, with nanotubes as the structure standing out as the most sensitive and most selective to ethanol. This paper also added data of Density Functional Theory calculations of the adsorption energies of NO_2 on α-V_2O_5 (011) clean and 3d transition metal (Cu, Mn, Ag, Sn) surfaces, revealing that incorporation of Ag could play a critical role in increasing the sensing effectiveness of V_2O_5 at low concentrations of NO_2 molecules.

This paper has reviewed hierarchical nano-layered V_2O_5 structures for gas sensing applications. Various morphologies and atomic structures, ranging from nanowires to thin films, were examined in terms of their gas detection capabilities, with discussion focused on target gases, operating concentrations, response, and recovery times. The analysis also highlighted that, among the reviewed

 doi:10.20944/preprints202602.0309.v1

structures, nanorods have been studied more extensively at room temperature—a desirable feature for energy-efficient practical applications.

It was found that ethanol and NO_2 are the most commonly targeted gases for these V_2O_5 nanostructures, with nanotubes emerging as a particularly sensitive and selective morphology for ethanol detection. Furthermore, this review incorporates original DFT calculations of the adsorption energies and adsorption energy per number of chemical molecules [145] of NO_2 on pristine and 3d transition metal (Cu, Mn, Ag, Sn, W)-doped α-V_2O_5 (011) surfaces. The results reveal that silver (Ag) doping significantly enhances adsorption energy, suggesting a critical role for Ag in improving the sensing effectiveness of V_2O_5, especially at low concentrations of NO_2.

References

1. Mane, A.A.; Suryawanshi, M.P.; Kim, J.H.; Moholkar, A.V., "Highly selective and sensitive response of 30.5 % of sprayed molybdenum trioxide (MoO3) nanobelts for nitrogen dioxide (NO2) gas detection," *Journal of Colloid and Interface Science,* vol. 483, pp. 220-231, 2016.
2. Davies, M.; Hobbs, F.; Davis, R., "Prevalence of left-ventricular systolic dysfunction and heart failure in the Echocardiographic Heart of England Screening study: a population based study," *Lancet.,* vol. 358, pp. 439-44, 2001.
3. Redfi eld, M.M.; Jacobsen, S.J.; Burnett, J.C.; Mahoney, D.W.; Bailey, K.R.; Rodeheffer, R.J., "Burden of systolic and diastolic ventricular dysfunction in the community: appreciating the scope of the heart failure epidemic.," *JAMA,* vol. 289, pp. 194-202, 2003.
4. Nazar, A.S.; Majeed, G.; Murrawat, A.; Muhammad, A.;, "Synthesis of Metal Oxide Semiconductor Nanostructures for Gas Sensors," *intechopen,* 2019.
5. Naderi, H.; Hajati, S.; Ghaedi, M.; Dashtian, K.; Sabzehmeidani, M.M., "Sensitive, selective and rapid ammonia-sensing by gold nanoparticle-sensitized V2O5/CuWO4 heterojunctions for exhaled breath analysis.," *Applied Surface Science,* vol. 501, p. 144270, 2020.
6. Roper, C.; Delgado, L.S.; Barrett, D.; Simonich, S.L.M.; Tanguay, R.L., "PM2.5 filter extraction methods: implications for chemical and toxicological analyses.," *Environ. Sci. Technol.,* vol. 53, pp. 434-442, 2018.
7. Roper, C.; Delgado, L.S.; Barrett, D.; Simonich, S.L.M.; Tanguay, R.L., "PM2.5 filter extraction methods: implications for chemical and toxicological analyses.," *Environ. Sci. Technol,* vol. 53, pp. 434-442, 2018.
8. Zhang, J.; Ouyang, Y.; Ye. Z.; Li. Q.; Lin, T.; Chen, Z.; Zhang, S., "Mixed-valence cobalt (II/III) metal–organic framework for ammonia sensing with naked-eye color switching.," *ACS Appl. Mater. Interfaces.,* vol. 10, pp. 27465-27471, 2018.
9. Heiland, G.; , "Zum Einfluß von Wasserstoff auf die elektrische Leitfähigkeit an der Oberfläche von Zinkoxydkristallen," *Phys,* vol. 148, pp. 15-27, 1957.
10. Jeun, J.H.; Kim, D.H.; Hong, S.H., " Synthesis of porous SnO2 foams on SiO2/Si substrate by electrochemical deposition and their gas sensing properties," *Sens. Actuators B,* vol. 161, pp. 784-790, 2012.
11. Liu, Y.; Hang, T.; Xie, Y.; Bao, Z.; Song, J.; Zhang, H.; Xie, E., "Effect of Mg doping on the hydrogen-sensing characteristics of ZnO thin films.," *Sens. Actuators B.,* vol. 160, pp. 266-270, 2011.
12. Hassan, K.; Chung, G., " Catalytically activated quantum size Pt/Pd bimetallic core-shell nanoparticles decorated on ZnO nanorod clusters for accelerated hydrogen gas detection," *Sens. Actuators B,* vol. 239, p. 824–833, 2017.
13. Perfecto, T.M.; Zito, C.A.; Volanti, D.P., "Design of nanostructured WO30.33H2O via combination of ultrasonic spray nozzle and microwave-assisted hydrothermal methods for enhancing isopropanol gas sensing at room temperature.," *Cryst. Eng. Comm.,* vol. 2733–2738, p. 19, 2017.

 doi:10.20944/preprints202602.0309.v1

14. Flak, D.; Braun, A.; Michalow, K.A.; Parlinska-Wojtan, J.W.M.; Graule, T.; Rekas, M., "Differences in electrophysical and gas sensing properties of flame spray synthesized Fe2O3 (γ-Fe2O3 and α-Fe2O3).," *J. Nanosci. Nanotechnol.,* vol. 12, p. 6401–6411, 2012.
15. Zakrzewska, K.; Radecka, M.; Rekas, M., "Effect of Nb, Cr, Sn additions on gas sensing properties of TiO2 thin.," *films. Thin Solid Films.,* vol. 310, pp. 161-166, 1997.
16. Lyson-Sypien, B.; Czapla, A.; Lubecka, M.; Gwizdz, P.; Schneider, K.; Zakrzewska, K.; Michalow, K.; Graule, T.; Reszka, A.; Rekas, M.; et al., "Nanopowders of chromium doped TiO2 for gas sensors.," *Sens. Actuators B.,* vol. 175, pp. 163-172, 2012.
17. Qin, Y.; Guangtao F.; Liu, K.; Ming, H., "Vanadium pentoxide hierarchical structure networks for high performance ethanol gas sensor with dual working temperature characteristic.," *Sensors and Actuators B.,* vol. 190, pp. 141-148, 2014.
18. Wonbong, C.; Nitin, C.; Gang, H.; Han, J.; Park, D.; Young, H.L., "Recent development of two-dimensional transition metal dichalcogenides and their applications.," *Materials Today.,* vol. 20, p. 116, 2017.
19. Eunji, L.; Young, S.Y.; Dong, J. K., "Two-Dimensional Transition Metal Dichalcogenides and Metal Oxide Hybrids for Gas Sensing.," *ACS Sens.,* vol. 3, pp. 2045-2060, 2018.
20. Liu, H.; Neal, A.T.; Zhu, Z.; Luo, Zhe.; Xu, X.; Toma´nek, D.; Ye, D.P., "Phosphorene: An Unexplored 2D Semiconductor with a High Hole Mobility.," *ACS NANO.,* vol. 8, pp. 4033-4041, 2014.
21. Akande, A. A.; Linganiso, E. CDhonge, B. P.; Rammutla, K. E.; Machatine, A.; Prinsloo, L.; Kunert, H.; Mwakikunga, B.W., "Phase evolution of vanadium oxides obtained through temperature programmed calcinations of ammonium vanadate in hydrogen atmosphere and their humidity.," *Materials Chemistry and Physics.,* vol. 151, pp. 206-214, 2015.
22. Rao M. C., "Vanadium Pentoxide Cathode Material for Fabrication of all Solid State Lithium-Ion Batteries- a Case Study.," *Research Journal of Recent sciences.,* vol. 2, pp. 67-73, 2013.
23. Reddy, I.N.; Sreedhar, A.; Reddy, C.V.; Cho, M.; Kim, D.; Shim, J., "Facile synthesis and characterization of V2O5 nanobelt bundles containing plasmonic Ag for photoelectrochemical water splitting under visible light irradiation.," *Ceram. Int.,* vol. 45, p. 23333–23340, 2019.
24. Kyoung Jin Choi, Ho Won Jang,, "One-Dimensional Oxide Nanostructures as Gas-Sensing Materials: Review and Issues," *sensors,* vol. 10, pp. 4083-4099, 2010.
25. Vahid Amiri, Hossein Roshan, Ali Mirzaei, and Mohammad Hossein Sheikhi, "A Review of Nanostructured Resistive-Based Vanadium Oxide Gas Sensors," *Chemosensors,* vol. 8, p. 105, 2020.
26. Bouzidi, A.; Benramdane, N.; Bresson, S.; Mathieu, C.; Desfeux, R.; Marssi, M.E., "X-ray and raman study of spray pyrolysed vanadium oxide thin films.," *Vib. Spectrosc.,* vol. 57, pp. 182-186, 2011.
27. Su, Q.; Lan, W.; Wang, Y.Y.; Liu, X.Q., "Structural characterization of β-v2o5 films prepared by dc reactive magnetron sputtering.," *Appl. Surf. Sci.,* vol. 255, p. 4177–4179, 2009.
28. Mwakikunga, B.W.; Sideras-Haddad, E.; Forbes, A.; Arendse, C.J., "Raman spectroscopy of WO3 nano-wires and thermo-chromism study of VO2 belts produced by ultrasonic spray and laser pyrolysis techniques Phys.," *Status Solidi.,* vol. 205, pp. 150-4, 2008.
29. Schneider, k.; Maziarz, W., "V2O5 Thin Films as Nitrogen Dioxide Sensors.," *sensors.,* vol. 18, p. 4177, 2018.
30. Eunji, L.; Young, S.Y.; Dong, J.K., "Two-Dimensional Transition Metal Dichalcogenides and Metal Oxide Hybrids for Gas Sensing.," *ACS Sens.,* vol. 3, pp. 2045-2060, 2018.
31. Mak, K.F.; Lee, C.; Hone, J.; Shan, J.; Heinz, T.F., "Atomically Thin MoS2.," *Phys. Rev. Lett.,* vol. 105, p. 136805, 2010.

 doi:10.20944/preprints202602.0309.v1

32. Liu, H.; Neal, A.T.; Zhu, Z.; Luo, Z.; Xu, X.; Tomanek, D.; Ye, P.D., "Phosphorene: An unexplored 2D semiconductor with a high hole mobility.," *ACS Nano,* vol. 8, pp. 4033-4041, 2014.
33. Liu, X.; Ma, T.; Pinna, N.; Zhang, J., "Two-Dimensional Nanostructured Materials for Gas Sensing.," *Adv. Funct. Mater.,* vol. 27, p. 1702168, 2017.
34. Joshi, N.; Hayasaka, T.; Liu, Y.; Liu, H.; Oliveira, O.N., Jr.; Lin, L., "A review on chemiresistive room temperature gas sensors based on metal oxidenanostructures, graphene and 2D transition metal dichalcogenides.," *Microchim. Acta.,* vol. 185, p. 213, 2018.
35. Mhlongo, G.H.; Motaung, D.E.; Nkosi, S.S.; Swart, H.C.; Gerald, F.; Malgas, K.T.; Mwakikunga, B.W., "Temperature-dependence on the structural, optical, and paramagnetic properties of ZnO nanostructures.," *Applied Surface Science.,* vol. 293, pp. 62-70, 2014.
36. Motuang, D. E.; Mhlongo, G. H.; Nkosi , S.S.; Malgas, G. F.; Mwakikunga, B. W.; Coetsee, E,; Swart, H. C.; Aballah, H. M. I.; Moyo, T.; Ray, S. S. , "Shape-Selective Dependence of Room Temperature Ferromagnetism Induced by Hierarchical ZnO Nanostructures.," *Applied material & interfaces.,* vol. 6, pp. 8981-8995, 2014.
37. Raseputuka, S.V.; Malwela, T.; Lemmer, Y.; Mervyn, B.; Mwakikunga, B.W., "The hierarchical nanostructured Co-doped WO3/carbon and their improved acetone sensing performance.," *Materials Science in Semiconductor Processing.,* vol. 117, p. 105157, 2020.
38. Xu, L.; Zeng, W.; Li, Y., "Synthesis of morphology and size-controllable SnO2 hierarchical structures and their gas-sensing performance.," *Applied Surface Science.,* vol. 457, pp. 1064-1071, 2018.
39. Xu, W.; Qiu, C.; Zhou, J.; Chen, Y., "Regulation of specific surface area of 3D flower-like WO3 hierarchical structures for gas sensing application.," *Ceramics International.,* vol. 46, p. 11372–11378, 2020.
40. Xu, L.; Zeng, W.; Li, Y., "Synthesis of morphology and size-controllable SnO 2 hierarchical structures and their gas-sensing performance.," *Applied Surface Science.,* vol. 457, pp. 1064-1071, 2018.
41. Lee, J.H., "Gas sensors using hierarchical and hollow oxide nanostructures: overview.," *Sens. Actuators B.,* vol. 140, pp. 319-336, 2009.
42. Bing, Y.; Zeng, Y.; Liu, C.; Qiao, L.; Sui, Y.; Zou, B.; Zheng, W.; Zou, G., "Assembly of hierarchical ZnSnO3 hollow microspheres from ultra-thin nanorods and the enhanced ethanol-sensing performances.," *Sensors and Actuators B: Chemical.,* vol. 190, pp. 370-377, 2014.
43. Zhu, L.; Zeng, W.; Li, Y., "New insight into gas sensing property of ZnO nanorods and nanosheets.," *Materials Letters.,* vol. 228, pp. 331-333, 2018.
44. Choi, K.; Kim, H.R.; Lee, J.H, "Enhanced CO sensing characteristics of hierarchical and hollow In2O3 microspheres.," *Sensors and Actuators B: Chemical.,* vol. 138, pp. 497-503, 2009.
45. W.J. Yan, M. Hu, P. Zeng, S.Y. Ma, M.D. Li, , "Room temperature NO2-sensing properties of WO3 nanoparticles/porous silicon,," *Appl. Surf. Sci.,* vol. 292, pp. 551-55, 2014.
46. Kanungo, J.; Saha, H.; Basu, S., "Pd sensitized porous silicon hydrogen sensor –influence of ZnO thin film.," *Sens. Actuators B: Chem.,* vol. 147, pp. 128-136, 2010.
47. Yan, D.; Hu, M.; Li, S.; Liang, J.; Wu, Y.; Ma, S., "Electrochemical deposition of ZnO nanostructures onto porous silicon and their enhanced gas sensing to NO2 at room temperature.," *Electrochim. Acta.,* vol. 115, pp. 297-305, 2014.
48. Yan, W.; Hu, M.; Wang, D.; Li, C., "Room temperature gas sensing properties of porous silicon/V2O5 nanorods composite.," *Applied Surface Science.,* vol. 346, pp. 216-222, 2015.
49. Pan, Z. W.; Dai, Z. R.; Wang, Z. L., "Lead oxide nanobelts and phase transformation induced by electron bean irradiation.," *APPLIED PHYSICS LETTERS.,* vol. 80, p. 2, 2002.

 doi:10.20944/preprints202602.0309.v1

50. Rane, AV.; Kanny, K.; Abitha, VK.; Thomas, S.;, "Methods for synthesis of nanoparticles and fabrication of nanocomposites.," *Elsevier Ltd.*, 2018.
51. Lui, J.; Wang, X.; Peng, Q.; Li, Y., "Vanadium Pentoxide Nanobelts: Highly Selective and Stable Ethanol Sensor Materials.," *Adv. mater.*, vol. 17, p. 6, 2005.
52. Liu, J.; Wang, X.; Peng, Q.; Li, Y., "Preparation and gas sensing properties of vanadium oxide nanobelts coated with semiconductor oxides.," *Sensors and Actuators B.*, vol. 115, pp. 481-487, 2006.
53. Liu, J.; Wang, X.; Peng, Q.; Li, Y., "Preparation and gas sensing properties of vanadium oxide nanobelts coated with semiconductor oxides.," *Sensors and Actuators B.*, vol. 115, pp. 481-487, 2006.
54. Shi, S.; Cao, M.; He, X.; Xie, H., "Surfactant-Assisted Hydrothermal Growth of Single-Crystalline Ultrahigh-Aspect-Ratio Vanadium Oxide Nanobelts.," *Crystal Growth & Design.*, vol. 7, p. 9, 2007.
55. Chen, H.; Di, J.; Wang, N.; Dong, H. ; Wu, J.; Zhao, Y., "Small," *small*, vol. 7, p. 1779, 2011.
56. Zeng, W.; Chen, W.; Li, Z.; Zhang, He.; Li. T., "Rapid and sensitive ethanol sensor based on hollow Au/V2O5 nanotubes via emulsion-electrospinning route.," *Materials Research Bulletin.*, vol. 65, pp. 157-162, 2015.
57. Liu, J.; Wang, X.; Peng, Q.; Li, Y., "Preparation and gas sensing properties of vanadium oxide nanobelts coated with semiconductor oxides.," *Sensors and Actuators B.*, vol. 115, pp. 481-487, 2006.
58. Fu,H.; Xie, H.;, "Hydrothermal synthesis of silver vanadium oxide (Ag0.35V2O5) nanobelts for sensing amines.," *Nanoscale Res Lett.*, vol. 10, p. 411, 2015.
59. Qiang, X.; Hu, M.; Zhou, L.; Liang, J., "Pd nanoparticles incorporated porous silicon/V2O5nanopillars and their enhanced p-type NO2-sensing properties at room temperature.," *Mater Lett.*, vol. 231, pp. 194-197, 2018.
60. Moshfegh, A. Z.; Ignatiev, A., *Thin Solid Films.*, vol. 198, p. 253, 1991.
61. Vernardou, D.; Paterakis , P.; Drosos, H.; Spanakis, E.; Povey, I.M.; Pemble, M.E.; Koudoumas, E.; Katsarakis, N., "A study of the electrochemical performance of vanadium oxide thin films grown by atmospheric pressure chemical vapour deposition.," *Solar Energy Materials & Solar Cells.*, vol. 95, p. 2842–2847, 2011.
62. Vernardou, D.; Paterakis, P.; Drosos, H.; Spanakis, E.; Povey, I.M.; Pemble, M.E.; Koudoumas, E.; Katsarakis,N., "A study of the electrochemical performance of vanadium oxide thin films grown by atmospheric pressure chemical vapour deposition," *Solar Energy Materials and Solar Cells*, vol. 95, pp. 2842-2847, 2011.
63. Gopalakrishnan, G.; Ramanathan, S., "Compositional and metal–insulator transition characteristics of sputtered vanadium oxide thin films on yttria-stabilized zirconia.," *Journal of Materials Science.*, vol. 46, pp. 5768-5774, 2011.
64. Givernaud, J.; Crunteanu, A.; Orlianges, J.C.; Pothier, A.; Champeaux, C.; Catherinot, A.; Blondy, P., "Microwave power limiting devices based on the semiconductor–metal transition in vanadium–dioxide thin films.," *IEEE Transactions on Microwave Theory and Techniques.*, pp. 2352-2361, 2010.
65. Ramana, C.V.; Smith, R.J.; Hussain, O.M.; Julien, C.M., "On the growth mechanism of pulsed-laser deposited vanadium oxide thin films.," *Materials Science and Engineering B.*, vol. 111, pp. 218-225, 2004.
66. Huotari, J.; Lappalainen, J.; Puustinen, A.; Spetz, L., "Gas sensing properties of pulsed laser deposited vanadium oxide thin films with various crystal structures.," *Sensors and Actuators B: Chemical.*, vol. 187, pp. 386-394, 2013.
67. Ramana, C.V.; Smith, R.J.; Hussain, O.M.; Julien, C.M., "On the growth mechanism of pulsed-laser deposited vanadium oxide thin films.," *Materials Science and Engineering B.*, vol. 111, pp. 218-225, 2004.

 doi:10.20944/preprints202602.0309.v1

68. Mane, AA.; Suryawanshi, M.P.; Kim, J.H.; Moholkar, A.V., "Superior selectivity and enhanced response characteristics of palladium sensitized vanadium pentoxide nanorods for detection of nitrogen dioxide gas.," *J Colloid Interface Sci.,* vol. 495, pp. 53-60, 2017.
69. Vahid, A.; Hossein, R.; Ali, M.; Mohammad, H.S., "A Review of Nanostructured Resistive-Based Vanadium Oxide Gas Sensors.," *Chemosensors.,* vol. 8, p. 105, 2020.
70. Wang, X.Z.; Qiu, S.; He, C.Z.; Lu, G.X.; Liu, W.; Liu, J.R., *RSC Adv,* vol. 3, p. 19002, 2013.
71. Schneider, K.; Lubecka, M.; Czapla, A., "V2O5 thin films for gas sensor applications.," *Sens. Actuators B: Chem.,* vol. 236, pp. 970-977, 2016.
72. Vijayakumar, y.;, "V2O5 nanofibers: potential contestant for high performance xylene sensor," *J. Alloy. Compd,* vol. 731, pp. 85-812, 2018.
73. Alrammouz, R.; Lazerges, M.; Pironon, J.; Bin Taher, I.; Randi, A.; Halfaya, Y.; Gautier, S., "V2O5 gas sensors: A review.," *Sensors and Actuators: A. Physical.,* vol. 332, p. 13179, 2021.
74. Rizzo, G.;, Arena, A.; Bonavita, A.; Donato, N.; neri, G.; Saitt, G., "Gasochromic response of nanocrystalline vanadium pentoxide films deposited from ethanol dispersions.," *Thin Solid Films,* vol. 518, pp. 7124-7127, 2010.
75. Schneider, K.; Lubecka, M.; Czapla, A., "VOx thin films for gas sensor applications.," *Procedia Engineering.,* vol. 120, pp. 1153-1157, 2015.
76. Yu, D.; Zhang, S.; Liu, D.; Zhou, X.; Xie, S.; Zhang, Q.; Liu, Y.; Cao, G. , "Effect of manganese doping on Li-ion intercalation properties of V2O5 films, J. Mater.," *Chem.,* vol. 20, p. 10841–10846, 2010.
77. Huotari, J.; Bjorklund, R.; Lappalainen, J; Lloyd Spetz, A.;, "Pulsed Laser Deposited Nanostructured Vanadium Oxide Thin Films Characterized as Ammonia Sensors," *Sensors and Actuators B: Chemical,* vol. 217, pp. 22-29, 2015.
78. Dhayal Raj, A.; Pazhanivel, T.; Suresh Kumar P.; Mangalaraj, D. Nataraj, D. Ponpandian, N., "Self assembled V2O5 nanorods for gas sensors.," *Current Applied Physics.,* vol. 10, pp. 531-537, 2010.
79. Ostermann, R.; Li, D.; Yin, Y.; Jesse, T.; Xia, M. Y., "V2O5 Nanorods on TiO2 Nanofibers: A New Class of Hierarchical Nanostructures Enabled by Electrospinning and Calcination.," *Nano Letters.,* vol. 6, pp. 1297-1302, 2006.
80. Huang, M.; Mao, S.; Feick, H.; Yan, H.; Wu, Y.; Kind, H.; Weber, E.; Russo, R.; Yang, P. D., *Science,* vol. 292, p. 1897, 2001.
81. Mane, A.A.; Suryawanshi, M.P.; Kim, J.H.; Moholkar, A.V. , "Superior selectivity and enhanced response characteristics of palladium sensitized vanadium pentoxide nanorods for detection of nitrogen dioxide gas.," *Journal of Colloid and Interface Science.,* vol. 495, pp. 53-60, 2017.
82. Nirav, J.; Takeshi, H.; Yumeng, L.; Huiliang, L.; Osvaldo, N.; Oliveira, J.R.; Liwei, L., "A review on chemiresistive room temperature gas sensors based on metal oxide nanostructures, graphene and 2D transition metal dichalcogenides.," *Microchim Acta.,* vol. 185, p. 213, 2018.
83. Abdul Hakim, S.; Liu, Y.; Lu, Y.; Chen, W., "Room temperature highly selective ethanol sensing behavior of hydrothermally prepared Te-V2O5 nanorod nanocomposites.," *Mater Sci Semicond Process.,* vol. 31, pp. 160-638, 2015.
84. Jimenez, V.M.; Espinos, J.P.; Gonzalez-Elipe A.R., "Effect of texture and annealing treatments in SnO and PdrSnO gas sensor materials.," *Sensors and Actuators B.,* vol. 61, pp. 23-32, 1999.
85. Ho, Y.K., "Characterization of gasochromic vanadium oxides films by X-ray absorption spectroscopy, 6th Int. Conf. Technol.," *Adv. Thin Films Surf. Coat.,* vol. 544, pp. 461-465, 2013.
86. Li, Y.; Huang, Z.; Rong, S., "A vanadium oxide nanotube-based nitric oxide gas sensor.," *Sens. Mater.,* vol. 18, p. 241–249, 2006.

 doi:10.20944/preprints202602.0309.v1

87. Dong, Y.; Wei, H.; Liu, W.; Liu, Q.; Zhang, W.; Yang, Y., "Template-free synthesis of V2O5 hierarchical nanosheet-assembled microspheres with excellent cycling stability.," *Journal of Power Sources.,* vol. 285, pp. 538-542, 2015.
88. Gibson, P.W.; Schreuder-Gibson, H.L.; Riven, D., *AIChE J.,* vol. 45, p. 190, 1999.
89. Katti, D.S.; Robinson, K.W.; Attawia, M.A.; Ko, F.K.; Laurencin, C.T., "Society for Biomaterials 28th Annual.," *Mtg Transactions.,* p. 143, 2002.
90. Muster, J.; Kim, G. T.; Krstic, V.; Park, J. G.; Park, Y. W.; Roth, S.; Burghard, M., *Adv. Mater.,* vol. 12, p. 420, 200.
91. Raible, I.; Burghard, M.; Schlecht, U.; Yasuda, A.; Vossmeyer, T., "V2O5 nanofibres: novel gas sensors with extremely high sensitivity and selectivity to amines.," *Sensors and Actuators B: Chemical.,* vol. 106, pp. 730-735, 2005.
92. Li, D.; McCann, J.T.; Xia, Y.N.; Marquez, M., "Electrospinning: a simple and versatile technique for producing ceramic nanofibers and nanotubes.," *J. Am. Ceram. Soc.,* vol. 89, pp. 1861-1869, 2006.
93. Li, D.; Xia, Y.N., "Electrospinning of nanofibers: reinventing the wheel.," *Adv. Mater.,* vol. 16, pp. 1151-1170, 2004.
94. Patil, J.V.; Mali, S.S.; Kamble, A.S., "a versatile technique for making of 1D growth of nanostructured nanofibers and its applications: an experimental approach.," *Appl Surf Sci.,* vol. 423, pp. 641-674, 2017.
95. Muster, J.; Kim, G.T.; Krstic, V.;. Park, J.G.; Park, Y.W.; Roth, S.; Burghard, M., "Electrical transport through individual vanadium pentoxide nanowires.," *Adv. Mater.,* vol. 12, pp. 420-424, 2000.
96. Modafferi, v., "Highly sensitive ammonia resistive sensor based on electrospun v2o5 fibers.," *Sens. Actuators B: chem,* vol. 163, pp. 61-68, 2012.
97. Feng, C,; Li, X.; Wang, c., "Facile synthesis benzene sensor based on V2O5-doped SnO2 nanofibers.," *RSC Adv.,* vol. 4, pp. 47549-47555, 2014.
98. Viswanathamurthi, P.; Bhattarai, N.; Kim ,H.Y.; Lee D.R., "Vanadium pentoxide nanofibers by electrospinning.," *Scripta Materialia.,* vol. 49, pp. 577-581, 2003.
99. Huang, M.H.; Wu, Y.Y.; Feick, H.; Tran, N.; Weber, E.; Yan, P.D., "Catalytic growth of zinc oxide nanowires by vapor transport.," *Adv. Mater.,* vol. 13, pp. 113-116, 2001.
100. Mounasamy, V.; Mani, G.K.; Ponnusamy, D.; Tsuchiya, K.; Prasad, A.K.; Madanagurusamy, S. , "Template-free synthesis of vanadium sesquioxide (V2O3) nanosheets and their room-temperature sensing performance.," *J. Mater. Chem. A.,* vol. 6, pp. 6402-6413., 2018.
101. Qin, Y.; Fan, G.; Liu, K.; Hu, M., "Vanadium pentoxide hierarchical structure networks for high performance ethanol gas sensor with dual working temperature characteristic.," *Sensors and Actuators B.,* vol. 190, pp. 141-148, 2014.
102. Pradhan, M.; Roy, A.; Sinha, A.K.; Sahoo, R.; Deb, D.; Pal, T., "Solid-state transformation of single precursor vanadium complex nanostructures to V2O5 and VO2 : catalytic activity of V2O5 for oxidative coupling of 2-naphthol.," *Dalton Trans.,* vol. 44, pp. 1889-1899, 2015.
103. Xu, Z.; Li, J. ; Qiao, X.; Huang, J.; Ouyang, H. , "V2O5 nanoflowers assembled by nanorods as cathode material for lithium-ion batteries.," *Micro & Nano Lett.,* vol. 10, pp. 686-688, 2015.
104. Tang, Y.; Rui, X.; Zhang, Y.; Lim, T.M.; Dong, Z.; Hng, H.H.; Chen, X.; Yan, Q.; Chen, Z. , "Vanadium pentoxide cathode materials for high-performance lithium-ion batteries enabled by a hierarchical nanoflower structure via an electrochemical process.," *J. Mater. Chem. A.,* vol. 1, pp. 82-88, 2013.
105. O'Dwyer, C.; Navas, D.; Lavayen, V.; Benavente, E.; Santa Ana, M.A.; Gonzalez, G.; Newcomb, S.B.; Sotomayor Torres, C.M., "Nano-urchin: the formation and structure of high-density spherical clusters of vanadium oxide nanotubes.," *Chem. Mater.,* vol. 18, pp. 3016-3022, 2006.

 doi:10.20944/preprints202602.0309.v1

106. Kaur, R.; Bhardwaj, S.K.; Kim, K.H.; Deep, A.; Vellingiri, K.; Kukkar, D., "Nano-materials for sensing of formaldehyde in air: principles, applications, and performance evaluation.," *Nano Res.,* vol. 12, pp. 225-246,, 2018.
107. Qin, Y.; Fan, G.; Liu, K.; Hu, M., , "Vanadium pentoxide hierarchical structure networks for high performance ethanol gas sensor with dual working temperature characteristic.," *Sensors Actuators B Chem,* vol. 190, pp. 141-148, 2014.
108. Vijayakumar, Y.; Mani, G.K.; Reddy, M.V.R.; Rayappan, J.B.B., , "Nanostructured flower like V2O5 thin films and its room temperature sensing characteristics," *Ceram Int,* vol. 41, pp. 2221-2227, 2015.
109. Vijayakumar, Y.; Mani, G.K.; Reddy, M.V.R.; Rayappan, J.B.B., , "Nanostructured flower like V2O5 thin films and its room temperature sensing characteristics," *Ceram Int,* vol. 41, p. 2221, 2015.
110. Yang, T.; Yu, H.; Xiao, B., , "Enhanced 1-butylamine gas sensing characteristics of flower-like V2O5 hierarchical architectures," *J Alloys Compd,* vol. 699, pp. 921-927, 2017.
111. Veena, M.; Ganesh, K.M.; Dhivya, P.; Kazuyoshi, T.; Reshma, P.R.; Arun, K.; Sridharan, M., "Investigation on CH4 sensing characteristics of hierarchical V2O5 nanoflowers operated at relatively low temperature using chemiresistive approach.," *Analytica Chimica Acta.,* vol. 1106, pp. 148-160, 2020.
112. Liu, J.; Wang, X.; Peng, Q.; Li, Y., "Preparation and gas sensing properties of vanadium oxide nanobelts coated with semiconductor oxides.," *Sens. Actuators B.,* vol. 115, pp. 481-487, 2006.
113. Yang, T.; Yu, H.; Xiao, B.; Li, Z.; Zhang, M., "Enhanced 1-butylamine gas sensing characteristics of flower-like v2o5 hierarchical architectures.," *J. Alloys Compd.,* vol. 699, p. 921–927, 2017.
114. Liu, J.; Wang, X.; Peng, Q.; Li, Y., "Vanadium Pentoxide Nanobelts:Highly Selective and Stable Ethanol Sensor Materials.," *Adv. Mater.,* vol. 17, pp. 764-767, 2005.
115. Liu, J.; Wang, X.; Peng, Q.; Li, Y., "Preparation and Gas Sensing Properties of Vanadium Oxide Nanobelts Coated with Semiconductor Oxides.," *Sens. Actuators, B.,* vol. 115, pp. 481-487, 2006.
116. Mai, L.; Xu, L.; Han, C.; Xu, X.; Luo, Y.; Zhao, S.; Zhao, Y., "Electrospun Ultralong Hierarchical Vanadium Oxide Nanowires with High Performance for Lithium Ion Batteries.," *Nano Lett.,* vol. 10, p. 4750–4755, 2010.
117. Ramgir, N.; Datta, N.; Kaur, M.; Kailasaganapathi, S.; Debnath, A. K.; Aswal, D. K.; Gupta, S. K., "Metal Oxide Nanowires for Chemiresistive Gas Sensors: Issues, Challenges and Prospects.," *Colloids Surf. A.,* vol. 439, pp. 101-106, 2013.
118. Ha Minh Tan, Chu Manh Hung,, Trinh Minh Ngoc, Hugo Nguyen, Nguyen Duc Hoa, Nguyen Van Duy, and Nguyen Van Hieu, "Novel Self-Heated Gas Sensors Using on-Chip Networked Nanowires with Ultralow Power Consumption," *ACS Applied Materials & Interfaces,* vol. 9, p. 6153−6162, 2017.
119. Jin W.; Yan, S., , "Enhancement of ethanol gas sensing response based on ordered V2O5 nanowire microyarns.," *Sensors Actuators B Chem,* vol. 206, pp. 284-290, 2015.
120. Mane, A.A.; Moholkar, A.V., , "Effect of film thickness on NO2 gas sensing properties of sprayed orthorhombic nanocrystalline V2O5 thin films," *Appl. Surf. Sci.,* vol. 416, pp. 511-520, 2017.
121. Yu H.Y.; Kang B.H.; Pi U.H., , "V2O5 nanowire-based nanoelectronic devices for helium detection," *Appl Phys Lett,* vol. 86, pp. 1-3, 2005.
122. Yu, H.Y.; Kang, B.H.; Pi, U.H.; Park, C.W.; Choi, S.Y.; Kim, G.T., , "V2O5 nanowire-based nanoelectronic devices for helium detection," *Appl. Phys. Lett.,* vol. 86, p. 25, 2006.
123. Yeh, B.Y.; Jian B.S.; Wang G.J.; Tseng W.J., , "CuO/V2O5 hybrid nanowires for highly sensitive and selective H2S gas sensor," *RSC Adv,* vol. 7, p. 49605–49612, 2017.

 doi:10.20944/preprints202602.0309.v1

124. Niranjan, R.; Niyanta, D.; Manmeet, K.S.; Kailasaganapathi, A.K.; Debnath, D.K.; Aswal, S.K.G., "Metal oxide nanowires for chemiresistive gas sensors: Issues, challenges and prospects.," *Colloids and Surfaces A: Physicochem. Eng. Aspects.,* vol. 439, pp. 101-116, 2013.
125. Wu, J.; Xing, X.; Zhu, Z.; Zheng, L.; Chen, J.; Wang, C.; Yang, D., "Electrospun hollow CuO modified V2O5 nano-string of pearls with improved acetone sensitivity.," *Chemical Physics Letters.,* vol. 727, pp. 19-24, 2019.
126. Muhammad Shahid, Imran Shakir, Seok-Jo Yang, Dae Joon Kang,, "Facile synthesis of core–shell SnO2/V2O5 nanowires and their efficient photocatalytic property," *Materials Chemistry and Physics,* vol. 124, pp. 619-622, 2010.
127. Saliman, A.; Reza, H.; Aghabozorg, S.K., "Synthesis and Characterization of Zr-Doped Vanadium Oxide Nanotubes.," *American Journal of Chemical Engineering.,* vol. 6, pp. 49-53, 2018.
128. Kanttcheva, M. , "Physical Chemistry Chemical Physics," pp. 3-43-3048, 2000.
129. Spahr, M.E.; Bitterli, P.; Nesper, R.; Muller, M.; Krumeich, F.;Nissen, H.U. , *Chem. Int. Ed.,* vol. 37, p. 1263, 1998.
130. Lavayen, V.; O'Dwyer, C.; Santa Ana, M.A.; Newcomb, S.B. Benavente, E.; González, G.; Sotomayor Torres, C.M.; , "Comparative structural–vibrational study of nano-urchin and nanorods of vanadium oxide," *Phys. Solid State (b),* vol. 243, p. 3285–3289, 2006.
131. O'Dwyer, C.; Lavayen, V.; Newcomb, S.B.; Benavente, E.; Santa Ana, M.A.; González, G; Sotomayor Torres, C.M., "Atomic layer structure of vanadium oxide nanotubes grown on nanourchin structures, Electrochem.," *Solid State Lett.,* vol. 10, p. A111–A114, 2007.
132. Liqiang Mai, Wen Chen, Qing Xu, Quanyao Zhu, Chunhua Han, Junfeng Peng, "Cost-saving synthesis of vanadium oxide nanotubes," *Solid State Communications,* vol. 126, p. 541–543, 2003.
133. Tenne, R.; Margulis, L,; Genut, M.; modes, G., *Nature,* vol. 360, p. 444, 1992.
134. Feldman, Y.; wasserman, E.; Srolouitz, D. j., Tenne, R., *Science,* vol. 267, p. 222, 1995.
135. Zeng, W.; Chen, W.; Li, Z.; Tianming, L., "Rapid and sensitive ethanol sensor based on hollow Au/V2O5 nanotubes via emulsion-electrospinning route.," *Materials Research Bulletin.,* vol. 65, pp. 157-162, 2015.
136. Wang, L.W.; Wang, S.R.; Xun, M.J.; Hu, X.J., , *Chem. Phys,* vol. 15, p. 17179, 2013.
137. Martin, E.; Saleta, J.C.; Troiani, H. E.; Guevara, S. R.; Sanchez, M.; Malta, R.T., "vanadium oxide hexadecyl amine multiwall nanotube, science direct.," pp. 333-336, 2007.
138. Shimizu, Y.; Egashira, M., "Basic aspects and challenges of semiconductor gas sensors.," *MRS Bull.,* vol. 24, pp. 18-24, 1999.
139. Li, Z.Y.; Wang, X.G.; Lin, T., *Mater. Chem. A,* vol. 2, p. 13655, 2014.
140. Wang, L.W.; Wang, S.R.; Xun, M.J.; Hu, X.J., *Phys. Chem. Chem. Phys,* vol. 15, p. 17179, 2013.
141. Yu, M.; Liu, X.; Wang, Y.; Zheng, Y.; Zhang, J.; Li, M.; Lan, W.; Su, Q., "Gas sensing properties of p-type semiconducting vanadium oxide nanotubes.," *Applied Surface Science.,* vol. 258, p. 9554–9558, 2012.
142. Zhang, X.; Zhao1, M.; Yan, S.; He, T.; Li, W.; Lin, X.; Xi, Z.; Wang, Z.; Liu, X.; Xia, Y., "First-principles study of ZnS nanostructures: nanotubes, nanowires and nanosheets.," *Nanotechnology.,* vol. 19, p. 305708, 2008.
143. Benaissa, N.; Benaissa , T.; Garmim, Z.; El Jouad, A.; Louardi, B.; Hartiti, M.; Monkade, A.; El Kenz, A.; , "Experimental and DFT TB-mBJ calculations studies of structural,morphological, electronic, optical and electrical properties of copper oxide thin films.," *Optical Materials.,* vol. 136, p. 113433, 2023.
144. Shahzad, K.; Anurag, S.; Rajneesh, C.M.; Shahid, K.; Piyush, D., "NH3and PH3adsorption through single walled ZnS nanotube:First principle insight.," *Chemical Physics Letters.,* vol. 636, pp. 103-109, 2015.

 doi:10.20944/preprints202602.0309.v1

145. Qin, Y.; Zhao, L.; Cui, M., "Ultrathin vanadium pentoxide nanobelt for ethanol-sensing applications: Experimental and ab initio study.," *Journal of Alloys and Compounds.,* vol. 735, pp. 1480-1487, 2018.
146. Akande, A.A.; Mosuanga, T.; Ouma, C.N.M.; Benecha, E.M. Tesfamicheal, T.; Rorof, K.; Machatine, A.G.J. Mwakikunga, B.W., "Ammonia gas sensing characteristics of V2O5 nanostructures: A combined experimental and ab initio density functional theory approach.," *Journal of Alloys and Compounds.,* vol. 821, p. 153565, 2020.
147. Prayut, B.; Wandee, R.; Banchob, W.; Chanukorn, T., "DFT investigation of NH3, PH3, and AsH3 adsorptions on Sc-, Ti-, V-,and Cr-doped single-walled carbon nanotubes.," *Applied Surface Science.,* vol. 400, p. 506–514, 2017.
148. Fu, H.; Xie, H.; Yang, X.; Xizhong, A.; Jiang, X.; Yu, A., "Hydrothermal Synthesis of Silver Vanadium Oxide (Ag0.35V2O5) Nanobelts for Sensing Amines.," *Nanoscale Research Letters.,* vol. 10, p. 411, 2015.